This manuscript was officially submitted for peer-review at *Tectonics* on October 8, 2018. Prior to this, the manuscript was uploaded to EarthArXiv for community 'peer-review' and comments were used to improve the quality of the manuscript. Please note that the manuscript is yet to be formally accepted for publication. Subsequent versions of this manuscript and the final published version may have slightly different contents. Please feel free to contact any of the authors. We look forward to your feedback.

Controls of basement fabric on rift coupling and development of normal fault geometries: Insights from the Rukwa - North Malawi Rift

Erin Heilman[1,2]

Folarin Kolawole[3]

Estella A. Atekwana[4]*

Micah Mayle[5]

[1]*Boone Pickens School of Geology*
Oklahoma State University
Stillwater, Oklahoma, USA

[2]*Jackson School of Geosciences*
University of Texas at Austin
Austin, Texas, USA

[3]*School of Geology & Geophysics*
University of Oklahoma
Norman, Oklahoma, USA

[4]*Department of Geological Sciences*
College of Earth, Ocean, and Environment
University of Delaware
Newark, Delaware, USA

[5]*Department of Geosciences*
Colorado State University
Fort Collins, Colorado, USA

**Corresponding author email: atekwana@udel.edu*

October 2018

Highlights

- To the SW, newfound strike-slip fault links the Rukwa and North Malawi Rift (RNMRS)
- To the NE, RNMRS border faults, intervening faults and volcanic centers are colinear
- RNMRS border faults and transfer structures align with pre-existing basement fabrics
- Basement fabrics guide the development of normal fault geometries and rift bifurcation
- Basement fabrics facilitate the coupling of the RMRS border faults and transfer structures

ABSTRACT

The Rukwa Rift and North Malawi Rift Segments (RNMRS) both define a major rift-oblique segment of the East African Rift System (EARS), and although the two young rifts show colinear approaching geometries, they are often regarded as discrete rifts due to the presence of the intervening Mbozi Block uplift located in-between. This problem has been complicated by the dominance of the Rungwe volcanic features along the northeastern boundary of the Mbozi Block and lack of distinct normal faults along the southwestern boundary of the block. Here, we investigate the coupling of discrete rift segments during the onset of continental rifting, modulated by the control of pre-existing basement fabrics on the development of the border fault geometries and linkage across the intra-rift transfer zone. We utilized the Shuttle Radar Topography Mission Digital Elevation Models (SRTM-DEM) to investigate the morphological architecture of the rift domains; and aeromagnetic data and SRTM-DEM to assess the relationships between the rift structures and the pre-existing basement fabric (in plan-view). Our results show that the present-day morphology of the RNMRS is characterized by along-rift alternation of rift shoulder polarity, characteristic of coupled rift segments. Careful interpretation of filtered aeromagnetic maps along

the northeastern and southwestern boundaries of the RNMRS reveal striking alignment of the rift-bounding faults with colinear NW-SE-trending pre-existing basement fabrics. We find that rift coupling along the northeastern boundary of the Mbozi Block transfer zone is accommodated by magmatism utilizing pre-existing fault systems, whereas, coupling along the southwestern boundary is accommodated by a new-found dextral strike-slip fault. Additionally, we show how the configuration of the pre-existing basement fabrics may influence the development of rectilinear or curvilinear normal fault geometries (plan-view) along the rifts, and the formation of basin-scale rift bifurcation around basement inter-rift transfer zones. In summary, we suggest that the structural continuation of the boundary faults along the RNMRS, and their alignment with colinear basement fabrics demonstrate the influence of structural inheritance on the coupling and amalgamation of approaching rift segments.

1. INTRODUCTION

Pre-existing basement fabrics are often major facilitators of continental rifting environments. Mechanically, they represent areas of structural weakness that can become reactivated and allow rifts to propagate preferentially along them (e.g., Daly et al., 1989). Several studies have documented the relationships between rift faults and the pre-existing basement fabrics (e.g., Wheeler and Karson, 1989; Kinabo et al., 2007, 2008; Taylor et al., 2011; Phillips et al., 2016; Kolawole et al., 2018; Siuda et al., 2018). Further, recent studies have assessed the 3-dimensional relationship between pre-existing basement thrusts and intra-rift normal faults, revealing the control of the pre-existing basement structures on the nucleation and strain distribution along the normal faults (e.g., Collanega et al., 2018). In the Cenozoic East African Rift System (EARS), which is divided into an Eastern, a Western and a Southwestern Branch (Fig. 1A), several zones of well-developed basement fabric influence rifting. One of the best recently-documented examples highlighting the influence of the Precambrian basement shear zones on rifting in eastern Africa is the role of the Mwembeshi Shear Zone on the development of the Luangwa Rift (Fig. 1A; Sarafian et al., 2018). It was demonstrated that the Mwembeshi Shear Zone acted as lithospheric conduit for fluids to migrate up the lithosphere, thus facilitating the weakening and subsequent initiation of the Luangwa rift in the Permo-Triassic.

However, the relationship between rift segments along the western branch of the EARS and the Precambrian shear zones is rather complex and warrants detailed and careful examination. For example, the Precambrian NW-trending Aswa shear zone resulted in the termination (rather than facilitation) of the northeastward propagation of the Albertine-Rhino graben which represents the northern-most segment of the Western Branch (Katumwehe et al., 2015) (Fig. 1A). On a basin scale, previous studies have also shown that pre-existing basement shear zones can influence the

localization of fault development (e.g., Phillips et al., 2016; Kolawole et al., 2018), and in fact control fault segmentation and across-basin strain transfer at later stages of rift development (e.g., Muirhead and Kattenhorn, 2018).

The border faults along large continental rift systems, e.g., the EARS, are typically ~100 km long (e.g., Foster et al., 1997; Lao-Davila et al., 2015), and the development of such large normal faults with complex segment linkage styles are yet to be fully understood (e.g., Fossen and Rotevatn, 2016; Gawthorpe et al., 2003; Rotevatn et al., 2018). However, since the interactions between the large normal faults within juvenile extensional tectonic settings lead to the systematic coupling of rift segments across transfer zones (e.g., Corti, 2012), border fault segmentation, geometries and continuity between rift segments can provide insight into the larger process of coupling between the segments of a rift system.

In this study, we focus on the Rukwa-North Malawi segment of the EARS, which is a major rift-oblique segment of the rift system and serves as the central segment of the system. For simplicity, we here-in refer to the Rukwa - Northern Malawi Rift segment of the East African Rift as the "RNMRS". This segment is composed of the Rukwa Rift basin, the North Malawi Rift basin and the Mbozi Block which represents the accommodation zone between the two rifts (Fig. 1B). We address the longstanding question of the role of long-lived pre-existing basement structures in the development of the trends and geometries of rift-bounding faults, leading to subsequent coupling of individual rift segments during the onset of continental rifting. We demonstrate that there is continuous structural connectivity along the boundaries of the RNMRS, modulated by reactivation of the Precambrian metamorphic fabrics, and show that the characteristic plan-view geometries of the rift-bounding faults are modulated by the configuration of the basement fabric.

2. GEOLOGIC SETTING

2.1. The Precambrian Domains

The Rukwa-North Malawi Rift Segment is located within the NW-trending Paleoproterozoic Ubendian orogenic belt which is sandwiched between the Archean Tanzanian craton in the northeast and the Bangweulu cratonic block to the southwest (Figs. 2A-B; Fritz et al., 2013). The Ubendian Belt is composed of different Precambrian terranes bounded by steep shear zones (Delvaux et al., 2012). These terranes contain granulite-facies metamorphic rocks (2100-2025 Ma), amphibolite-facies metamorphic rocks and granitoids (1960-1800 Ma) that have undergone dextral strike-slip shearing and granitic plutons (1090-1120 Ma), (Fritz et al., 2013). The Paleoproterozoic Usagaran orogenic belt that extends NE-SW perpendicular to the Ubendian orogenic belt in southern Tanzania, is composed of eclogites (~2000 Ma), volcano-sedimentary cover with some low-grade metamorphism (~1920 Ma), and granitoids and granitoid gneisses (1900-1730 Ma) (Fritz et al., 2013). The Usagaran and Ubendian orogenic belts resulted from collision with the Tanzania craton, where the Usagaran orogenic belt was thrust onto the craton and the Ubendian orogenic belt was accreted along the craton's margin because of strike-slip motion (Daly, 1988; Lenoir et al., 1994). The Ubendian Belt was reactivated several times, preserving geochronologic, and petrographic and geochemical evidences of successive terrane accretion (e.g., Lenoir et al., 1994; Boniface and Schenk, 2012; Boniface et al., 2012). Known terranes within the Ubendian Belt are separated by shear zones which include the Mughese Shear Zone and the Mtose Shear Zone (Fig. 2; Daly, 1988; Delvaux et al., 2012), where the Chisi Suture Zone represents the major suture zone between the Precambrian Tanzania Craton and Bangweulu Block (Boniface and Schenk, 2012). Recent studies have highlighted the role of these shear zones in fault development (e.g., Morley, 2010; Delvaux et al., 2012; Kolawole et al., 2018) and the

distribution of seismicity in southern Tanzania and northern Malawi (Dawson et al. 2017; Kolawole et al., 2018).

2.2. The Rukwa Rift, Northern Malawi Rift, and the Mbozi Block accommodation zone (RNMRS)

The RNMRS evolved during the Permo-Triassic episode of rifting that affected southern and eastern Africa, also known as Karoo rifting (Chorowicz, 2005). Outcrops of Karoo sediments have been mapped along the southern end of the Rukwa Rift (Figure 2) and the northern section of the North Malawi Rift Basin (Kilembe and Rosendahl, 1992). These sediments lie unconformably over the Precambrian basement and consist mainly of sandstone, shale, and coal and thicken towards the border faults providing evidence for reactivation of synthetic faulting in the Permo-Triassic (Morley, 1992; Delvaux et al., 1992).

Cenozoic rifting began in the Upper Miocene, characterized by normal faulting and basin subsidence with the diagenesis of Red Sandstones and Lake Bed Sediments (Delvaux and Hanon, 1991). Additional subsidence occurred after the deposition of these packages, and in different directions, evidenced by the drag orientations of sediment packages on the faults (Kilembe and Rosendahl, 1992). The Cenozoic rifting featured the reactivation of older faults as seen in seismic profiles of the Rukwa Rift in which the faults are mostly contiguous from Karoo sediments to Red Sandstones to Lake Beds (Kervyn et al., 2006). The present-day tectonic activity in the RNMRS consists of limited volcanic eruptions, minor seismicity in the Mbozi Block region, and continued sedimentation in the Rukwa and North Malawi basins (Delvaux and Hanon, 1991).

The present-day architecture of the RNMRS consists of the Rukwa Rift to the northwest of the segment, with the Lupa Fault (generally considered the border fault) bounding it to the northeast and the Ufipa Fault to the SW (Fig. 1B). Towards the southeastern end of the Rukwa

Rift. It bifurcates around the Mbozi Block forming the Songwe Trough (ST) to the northeast and the Musangano Trough (MT) to the southwest. The Mbozi Block transitions into the North Malawi Rift (also known as the North Basin) which represents the southeastern end of the RNMRS and it consists of a half-graben, bounded to the northeast by the Livingstone Fault (Fig. 1B). The Mbozi Block is referred to as an accommodation zone because it is thought to accommodate and transfer relative strain between the Rukwa and North Malawi Rift Basins (Delvaux and Hanon, 1993)

The Mbozi is a mass of Precambrian basement that is composed of Meta-basites and intermediate granulites and quartzites of the Mbozi Terrane (Daly, 1988) and is bounded to the southwestern by the Mughese Shear Zone (Fig. 2B), and overlain on the northeast by the volcanic deposits of the Rungwe Volcanic Province (RVP). The RVP is a ~1500 km^2 area of volcanic rocks and structures that evolved ca. 9 Ma (e.g., Fontijn et al., 2012), and a strong tectonic control on the localization of volcanic centers have been inferred (e.g., Fontijn et al., 2010, 2012). To the northeast of the RVP, a poorly defined NE-trending rift basin occurs, known as the "Usangu Basin", where Permo-Triassic to Recent sedimentary rocks overlie the Precambrian basement (Mbede, 2002).

The crustal thickness beneath the Rukwa Rift is ~37.5 km (Kim et al., 2009), but varies between ~33 km and ~39 km along the rift shoulder (Ufipa Plateau) (Hodgson et al., 2017), and increases slightly to 41.1–42.1 km in the northwestern-most part of the rift where the rifting is minimal. These suggest that overall, the crustal thinning beneath the rift has been minimal but may be slightly more beneath the Songwe Trough (Njinju et al., 2018). Camelbeeck and Iranga (1996) estimated ~42 km crustal thickness beneath the Songwe Trough. Whereas, an average crustal thickness of 39 km has been estimated for the Rungwe Volcanic Province, ~37-39 km for the North

231 Malawi Rift, and 38-42 km for the Proterozoic terrains surrounding the North Malawi Rift
232 (Borrego et al., 2016; Njinju et al., 2018).
233
234 *2.3. Kinematics of the RNMRS*
235 The mode of opening of the Rukwa Rift – Northern Malawi Rift segment is controversial. Overall,
236 two models have been proposed. One of the models advocates for orthogonal rifting due to the
237 dominance of NW-trending pre-existing basement fabric in the region, which resulted in the
238 rotation of the E-W directed regional extension into NE-SW, thus producing NW-striking normal
239 faults (e.g., Delvaux et al., 1992; Morley, 2010; Delvaux et al., 2012). The other model argues for
240 oblique extension primarily due to the obliqueness of the rift segment to the E-W directed
241 extension, thus resulting in the development of NW-trending dextral strike-slip faults (e.g.,
242 Chorowicz, 1989; Daly et al., 1989; Wheeler and Karson, 1994; Kervyn et al., 2006; Mortimer et
243 al., 2007). Both models are based on observations from only the Rukwa Rift and North Malawi
244 Rifts, and did not consider the kinematics of brittle structures along the Mbozi Block
245 accommodation zone.
246
247 **3.0 MATERIAL AND METHODS**
248 In this study, we carried out detailed mapping of exposed and buried fault segments within the
249 RNMRS. We utilized Shuttle Radar Topography Mission (SRTM) Digital Elevation Model
250 (DEM) to locate surface expressions of faults; and filtered aeromagnetic data to map the plan-view
251 trace of basement faults and metamorphic fabrics.
252
253 *3.1. SRTM DEM Data*

We extracted topographical profiles along the length of the rift from the SRTM DEM data to investigate surface morphology of the rift segments which could provide insight into the evolving nature of the rift architecture along the RNMRS.

3.2. Aeromagnetic Data

We combined three separate aeromagnetic surveys consisting of data acquired over northeastern Zambia, southern Tanzania and Northern Malawi. The Tanzania survey was collected between 1977-1980 with flight height of 200 m and a flight line spacing of 1 km. The Zambia survey was collected between 1973-1976 with a flight height of 150 m and a flight line spacing of 800-1000 m. The Malawi survey was carried out in 2013 with a flight height of 80 m, a flight line spacing of 250 m. Before merging the three surveys, we first corrected for the skewness of the data by reducing each of them to the magnetic pole (RTP). The RTP correction normalizes the magnetic field to the magnetic field at the pole so the anomalies retain their correct strike and shape, allowing the magnetic data to be interpreted as geologic structures (Baranov, 1957; Silva, 1986). Afterwards, we applied upward-continuation (Henderson and Zeitz, 1949) of 120 m to the RTP-corrected Malawi data, 50 m to the Zambia data in order to mathematically normalize the three datasets to a 200 m observational height. We then merged the three surveys into a single aeromagnetic grid file. Further, we applied the vertical derivative (VDR) filter to the merged data in order to enhance magnetic gradients associated with possible basement faults and basement metamorphic fabrics (Salem et al., 2008).

The vertical derivative edge filter has been very effective in the mapping of plan-view trace of buried active faults from aeromagnetic data in different parts of the EARS (Kinabo et al., 2007, 2008; Kolawole et al., 2017, 2018). Excluding the Rungwe Volcanic Province (RVP; Figure 3)

where volcanic materials overlie the crystalline basement, there is no information on the presence of basaltic rocks along the fault segments interpreted in this study. Therefore, we assume induced magnetization as the primary source of magnetization, except in the Rungwe Volcanic Province (RVP) where volcanic deposits are present. However, we do not have information on remanent magnetization in the RVP at this time. Due to the higher spatial resolution of the Malawi aeromagnetic data (62 m grid cell size) compared to those covering Zambia (225 m grid cell size) and Tanzania (250 m grid cell size), the magnetic anomalies are most significantly better resolved in the Malawi part of the filtered aeromagnetic maps.

4.0 RESULTS

4.1. Variation in rift morphology from topographic profiles

We examined fifteen rift-orthogonal topographic profiles (spaced at 40 km) along the RNMRS (Fig. 1B) to understand the overall along-strike variation in rift morphology. The investigation of rift dynamics by careful analyses of the topographic structures has provided important information on the subsurface architecture of rift systems (e.g., Pik et al., 2008; Wichura et al., 2011; Lao-Davila et al., 2015). Our morphological assessments focus on the variation in the scarp-heights (relief above the surface) of exposed normal faults along the RMNRS. This provides the minimum estimate of the relative vertical displacements of the faults at the point of assessment, hence the term ‘exposed minimum vertical displacement’ (EMVD) (Lao-Davila et al., 2015).

Profile 1 (Fig. 3), obtained at the northern tip of the Rukwa Rift shows no pronounced fault scarps, and the slight topographic high between Lake Tanganyika and Ufipa Fault represents the northernmost tip of the Ufipa Plateau. In Profile 2, the surface morphology of the rift shows sharp topographic gradients bounding the Rukwa Rift Valley. These topographic gradients correspond

to the scarps of the Ufipa Fault (600 m) and the Lupa Fault (750 m). In this northern part of the Rukwa Rift, the Ufipa and Lupa Faults have comparable scarp heights, thus illustrating a typical graben structure. In Profile 3, the rift structure changes into a half-graben surface morphology with the Ufipa Fault having a significantly higher escarpment than the Lupa Fault (~900 m difference). Profiles 4 to 7 show the same half-graben morphology for the Rukwa Rift as in Profile 3; however, we observe that the Ufipa Fault scarp is much higher than the topography of the Ufipa Plateau to its west along Profile 4.

Along Profiles 6 and 7, we observe that the Ufipa Fault scarp is lower than in the northern profiles (Profiles 1-5) and that the Lupa Fault scarp is also higher than in the northern profiles. In Profile 7, the Rukwa Rift splits into two basins separated by the Mbozi Block such that the west basin (Musangano Trough) is bound by the Ufipa Fault to the southwest, and the east basin (Songwe Trough) is bound by the Lupa Fault to the northeast. Profiles 7 to 9 shows a continuous southeastward decrease in the scarp heights of the Ufipa and Lupa Faults; and although the Ufipa Fault scarp is still visible south of the Mbozi Block along Profile 9, the Lupa Fault scarp is significantly diminished. Profile 9 shows a gentle topographic transition from the Musangano Trough to the Mbozi Block, but to the northeast of the Mbozi Block, the topography spikes abruptly, representing the northern limits of the Rungwe Volcanic Province (RVP). In Profile 10, the Ufipa Fault bounds what appears to be the southernmost extent of the Musangano Trough, while the uplifted Mbozi – RVP domain dominates the terrain and drops off into the Usangu Trough to the northeast. Profile 11 transects the northernmost tip of the North Malawi Rift, where the RVP (bounded to the northeast by the Livingstone Fault scarp) represents the most dominant structure in the terrain and the entire topography of the Mbozi Block and areas to its southwest are relatively lower.

Profiles 12 and 13 illustrate half-graben morphologies for the North Malawi Rift (North Basin) with the Livingstone Fault (northeast bounding fault) dominating the topography. Profile 14 transects the transfer zone between the North and Usisya Basins of the Malawi Rift showing both the Livingstone border fault to the northeast and the Nyika Plateau to the southwest. Profile 15 which transects the Usisya Basin describes a half-graben surface morphology but in which the rift bounding fault is located on the southwest.

4.2. Aeromagnetic lineaments and basement fabric

The RTP merged (Fig. 4A) and edge-enhanced (Fig. 4B) aeromagnetic maps over the RNMRS provide a continuous plan-view image of the basement structures along the rift segment. Although the Malawi part of the merged data has the highest resolution, the moderate resolution of the Tanzania and Zambia parts of the data allows for considerable delineation of the trends of magnetic anomalies. Overall, the areas of basement exposures exhibit high amplitude, high frequency and short wavelength magnetic anomalies that delineate lineaments of interpretable trends (e.g., Kolawole et al., 2018). The high frequency lineaments can be easily observed on the rift shoulders of the Rukwa and North Malawi Rifts (Fig. 4B), and are commonly truncated at the rift margins by the rift-bounding faults (black arrows in Fig. 4B).

Within the rift valleys where sedimentary rocks overlie the deeply-buried basement rocks, the detailed magnetic fabric of the basement becomes suppressed such that gradients in the magnetic data could correspond to fault offset within the magnetic source (e.g., Grauch and Hudson, 2007, 2011; Kolawole et al., 2018) or remnants of the suppressed magnetic foliation of the source (Kolawole et al., 2018). In the study area, the magnetic anomalies within the rift basins are dominated by relatively lower amplitude, longer wavelength and lower frequency anomalies.

346

347 *4.3. SRTM DEM Fault trends and Aeromagnetic lineaments*

348 We compare the along-axis geometry of the rift-bounding faults (from SRTM DEM) with the
349 metamorphic fabric (in plan view) of the host basement rocks along the rift shoulders (from filtered
350 aeromagnetic data) (Figs. 5-11). Figures 5-9 focus on the southwestern boundary of the RNMRS,
351 consisting of the Ufipa Fault of the Rukwa Rift, the southwestern boundary of the Mbozi Block
352 and the southwestern boundary faults of the North Malawi Rift. Whereas, Figures 10 and 11 focus
353 on the northeastern boundary of the RNMRS, consisting of the Lupa Fault of Rukwa Rift, the
354 northeastern boundary of the Mbozi Block (i.e. the Rungwe Volcanic Province) and the
355 Livingstone Fault of the North Malawi Rift. We constrain our identification of the Precambrian
356 terranes and strike of their fabrics with previous field studies of the Precambrian basement along
357 the RNMRS (e.g., Daly, 1988; Wheeler and Karson, 1989; Lenoir et al., 1994; Theunissen et al.,
358 1996; Boven et al., 1999; Fernandez-Alonso et al., 2001; Ring et al., 2002; Boniface and Schenk,
359 2012; Delvaux et al., 2012, Lawley et al., 2013; Kolawole et al., 2018). Overall, within the study
360 area, we observe that the basement fabrics exhibit two styles, (1) discrete fabrics which include
361 isolated magnetic lineaments of strong amplitude; and (2) distributed fabrics which encompass
362 fabric sets of multiple medium-to-low amplitude magnetic lineaments as distributed fabrics.

363

364 *4.3.1. Southwestern boundary of the RNMRS*

365 In the northernmost part of SW Rukwa Rift (Chisi area) (Figs. 5A-C), we observe curvilinear fault
366 geometries that follow Precambrian fabric (e.g., Ufipa, Chisi, Kalambo and Kanda Faults). In the
367 Chisi area, the Rukwa Rift border fault consists of the Northern Ufipa Fault segment and the Chisi
368 Fault segment. The tip of the Northern Ufipa Fault segment terminates against the WNW-ESE

Chisi Fault at a high angle (Fig. 5A). The Chisi Fault aligns with a strong WNW-ESE magnetic-high lineament (discrete fabric) (Fig. 5B-C) consistent with the Chisi Suture Zone, which extends eastward into the rift basin (Theunissen et al., 1996; Boven et al., 1999; Boniface and Schenk, 2012; Fig. 2B). Also, the truncated Ufipa Fault segment aligns with the Ufipa Terrane basement fabrics (distributed fabrics). The North Ufipa Fault and Chisi Fault link at a very high angle to form a salient that point basinward (the Chisi Salient).

In the central part of the Ufipa Fault (Figs. 6A-C), the fault segments also exhibit curvilinear geometries and the hard linkage of major fault segments occur at high angles (e.g., Kwera relay ramp). The Kwera relay ramp is the largest relay zone along the Ufipa Fault. To the north of the Kwera relay ramp, the fault trends parallel to a magnetic lineament (discrete fabric) that is located to its east, whereas, to the west of this fault segment, the basement is characterized by two cross-cutting sets (NNW-SSE and NW-SE) of distributed fabrics. The NNW-SSE set represent the fabrics of the Ufipa Terrane, but the origin NW-SE is unknown at this time. The Ufipa Fault segments appear to follow the NNW-SSE basement fabrics but side-steps by means of short fault segments that align with the NW-SE fabric set. To the south of the relay ramp, the Ufipa Fault strikes parallel to the Mughese Shear Zone fabric which is colinear with the NNW-SSE set.

Towards the southern part of the Ufipa Fault, in Figures 7A-C, we observe that the Ufipa Fault segments exhibit rectilinear geometries such that it is difficult to delineate fault bends that could correspond to breached relay ramps. In addition, we observe a stronger alignment of the Ufipa Fault segments with the Mughese Shear Zone fabric within the area. To the east of the Ufipa Fault, a fault that strikes parallel to the Ufipa Fault separates the Musangano Trough from the Mbozi Block. The Mbozi basement is characterized by metamorphic fabrics that strike

WNW-ESE to NW-SE, oblique to the fault but in which subtle bends in the fault trend align with the basement fabric.

In the southern part of the Ufipa Fault (Figs. 8A-C), the fault is characterized by two segments. One of the segments represents a rectilinear southward continuation of the Ufipa Fault and is bounded to the east by a linear ridge that separates it from the Musangano Trough (see "Mughese Fault" segment at Tunduma in Figs. 8A-C). The other segment splays away from the former and delineates a curvilinear geometry that looks like those in the northern and central segments of the Ufipa Fault; this curvilinear segment bounds the southernmost part of the Musangano Trough (see "Ufipa Fault" in Figs. 8A-C). Around Kaseye town (see Fig. 8A), the basement is partially buried and more deeply buried around Chitipa to the south. The continuation of the Ufipa Fault is only evident in the aeromagnetic data as a strong magnetic-low lineament that is bounded by bands of magnetic-high lineaments (see magnetic fabrics around Kaseye town in Fig. 8B). Within the Kaseye area, the NW-striking Mughese Shear Zone fabrics are truncated by a discrete N-S trending magnetic-high lineament (see area within purple rectangle in Fig 8C). The magnetic-low lineament that projects as a southward continuation of the Ufipa Fault persists along the Mughese Shear Zone fabric into the Karonga area of the North Basin of Malawi Rift where the Mughese Shear Zone is abruptly truncated by the Karonga Fault (KF in Fig. 8C). The Mbozi Terrane fabric strike NW-SE, at low angles to the trend of the Mughese Shear Zone.

Detailed analyses of the onshore faults along the hinge zone of the Northern Malawi Rift (Karonga area) are well documented in Kolawole et al. (2018). Major onshore hinge zone faults include the Karonga Fault (KF), St. Mary Fault (SMF), Kaporo Fault (KPF), Lupaso Fault (LF), Katesula Fault (KTF) and the Mbiri Fault (Figs. 9A-C). Although the Karonga Fault cuts the basement fabric, several basement-rooted buried fault segments along the rift margin align with

415 the fabric of the Mughese Shear Zone (Kolawole et al., 2018). It is interesting to note that
416 the Mbiri Fault, the longest fault (and potentially has the largest throw?) along the rift margin is
417 sub-parallel to the strike of the continuation of the Ufipa Fault into the area ("Mughese Fault" in
418 Fig. 9C). Although segments of the Mbiri Fault appear to align with the Mughese Shear
419 Zone fabic, it is not clear if the fault reactivated the southwestern boundary of the shear zone or if
420 the fault partially aligns with the fabric of the shear zone. However, we observe that for the most
421 part, the side-steps along the Mbiri Fault align with the basement fabric.
422
423 *4.3.2. Northeastern boundary of the RNMRS*
424 In the northern part of the Lupa Fault, the fault trend defines long, rectilinear segments (Fig. 10A)
425 and aligns with the Katuma Terrane, similar to those observed in the southern part of
426 the Ufipa Fault where faults align with the trend of the Ufipa Terrane (Fig. 7). Although, the E-W
427 trending fabric of the Usagaran Orogenic Belt dominates the aeromagnetic data along the
428 northeastern Rukwa Rift shoulder (Fig. 10B), we also observe that closer to the Lupa Fault scarp,
429 there are some lineaments that align with the fault. To the southwest of the Lupa Fault (within the
430 rift valley), a strong magnetic-high lineament which correspond to the Chisi Suture Zone (see
431 onshore continuation and outcrop of the shear zone in Fig. 5), strike sub-parallel to the trend of the
432 Lupa Fault, but deviates more significantly southwards (Figs. 4B and 10).
433 The southern part of the Lupa Fault (between the Katuma Terrane and the Rungwe
434 Volcanic Province) is characterized by curvilinear fault segments (Fig. 10 and 11). The Lupa
435 Terrane fabrics are oriented WNW-ESE, oblique to the Lupa Fault trend (Figs. 11A-C). However,
436 subtle steps along the curvilinear fault segments align with the Lupa Terrane fabrics.

In the Rungwe Volcanic Province (RVP), the magnetic lineaments strike NW-SE (Fig. 11B), similar to those of the Mbozi Terrane (8B and C), and are truncated to the west by a strong NNW-striking magnetic high lineament (white arrows in Fig. 11B). Furthermore, we observe that the volcanic centers align with NNW-striking magnetic gradient superimposed on the NW-striking fabrics (black arrows in Fig. 11B). South of the Rungwe Volcanic Province, segments of the Livingstone Fault system describe rectilinear geometries and align with strong magnetic-high lineaments (shear zone?) in the Upangwa Terrane.

5.0 DISCUSSION

5.1. Rift architecture

The present morphology of the RNMRS reflects the result of multiple episodes of rifting that have affected this part of eastern Africa i.e. a Permo-Triassic rifting episode (Karoo), a Cretaceous episode and the ongoing Cenozoic rifting episode (e.g., Castaing, 1991; Morley et al., 1992). The Rukwa Rift has been described as both a graben (e.g., Zhao et al., 1997) and half-graben (e.g., Kilembe and Rosendahl, 1992) bounded by the oppositely-dipping Ufipa and Lupa normal faults. The Lupa Fault is commonly regarded as the major border fault of the Rukwa Rift due to its larger throw of ~7 km (Peirce and Lipkov, 1988) relative to the Ufipa Fault (Fig. 12); however, it has also been shown that the Cretaceous and Cenozoic sediments in the rift thicken towards both faults (Fig. 12; Morley et al., 1992; Zhao et al., 1997). In this study, our topographical assessments (Fig. 3, profiles 1-7) show that the scarp height of the Ufipa Fault consistently exceeds that of the Lupa Fault through-out the rift segment, thus suggesting significant footwall uplift along the Ufipa Fault.

The significantly lower scarp-height of the Lupa Fault suggests either that it has not been very active in Cenozoic times or that it has been heavily eroded since the cessation of Mesozoic

rifting. However, based on these observations, we interpret that in the earlier rifting episodes (especially in the Permo-Triassic Karoo episode), the Lupa Fault played the role of the major border fault such that the basin defines a typical half-graben geometry; but in the present Cenozoic phase of rifting, the Ufipa Fault appear to have been preferentially accommodating more strain. Therefore, we suggest that the Rukwa Rift is possibly transitioning into an asymmetric-graben geometry. An asymmetric-graben is a graben with EMVD greater on one border fault compared to the other one, such that the basin polarity has shifted to the fault with the greater 'exposed minimum vertical displacement' (EMVD) (Lao-Davila et al., 2015). The implications of the present Rukwa Rift morphology on the Lupa Fault may reflect temporal and spatial migration of strain accommodation from a previously dominant border fault into another one that has been previously less-dominant. This could possibly be explained by the Scholz and Contreras (1998) suggestion that when a rift-bounding fault attains some limiting offset, motion on the fault will cease, and strain will be transferred to a new fault.

5.2. The Southwestern Boundary of the RNMRS and relationships with Precambrian Basement Fabric

In the Chisi area, the Northern Ufipa Fault segment terminates against the Chisi Suture Zone along which the Chisi Fault segment developed. The termination of the Ufipa Fault at its intersection with this shear zone exemplifies one of the roles of pre-existing basement structures as temporal and/or spatial mechanical 'barriers' that arrest and delimit the continuous lateral propagation of a fault. Several studies on fracture propagation have demonstrated that fractures are principally bifurcated, blunted, and/or arrested when they intersect discontinuities, stress barriers and/or rock layers of significantly-contrasting mechanical properties along their path of propagation (e.g.,

Helgeson and Aydin, 1991; Gudmundsson and Brenner, 2001; Zhang et al., 2007; Zhang and Jeffrey, 2008). Other examples of normal fault termination at long-lived basement shear zones include the case of the Albertine-Rhino Graben terminating at the Aswa Shear Zone (Katumwehe et al., 2015) and the Okavango Rift border faults against the Sekaka Shear Zone (Modisi et al., 2000). We suggest that both the reactivation of the Chisi Suture Zone into the Chisi Fault and termination of fault segments at the shear zone demonstrate the strong influence of the Chisi Suture Zone on the development of this part of the Rukwa Rift.

Although the northern segments of the Ufipa Fault align with the basement fabrics (Fig. 5B-C) and the southern segments show even stronger alignment with the NNW-SSE fabrics of the Ufipa Terrane and/or Mughese Shear Zone (Fig. 7), we find that the central segments of the fault show only partial alignment with this basement fabric (Fig. 6A-C). These observations imply that, although the Ufipa Fault is thought to have largely propagated along the Mughese Shear Zone (Fig. 2; Delvaux et al., 2012), there is stronger control of the Mughese Shear Zone and Ufipa Terrane fabrics on the fault development along its northern and southern segments than in the central part. We suggest that the partial control of these NNW-SSE fabrics on the central Ufipa Fault segments is due to the occurrence of a NW-SE basement fabric set on the Mughese Shear Zone and Ufipa Terrane fabric (Fig. 6). This may also explain the localization of the largest relay zone along the Ufipa Fault at its central segment.

The Tunduma-Kaseye area of Malawi, through the Misuku Mountains (Fig. 8A) constitute the southern boundary of the Mbozi Block. Although, the SRTM DEM shows that the sub-aerial expression of the Ufipa Fault dies out roughly mid-way between Tunduma and Kaseye, the filtered aeromagnetic data reveals that in the subsurface, the fault continues across the Kaseye-Chitipa area as a distinct magnetic-low lineament that bounds the Mughese Shear Zone to the south and runs

506 southeastwards into the Karonga area (Fig. 8B). Upon closer observation of the continuation of
507 this strong magnetic-low lineament in the Kaseye-Chitipa area, we find that it cuts-across and
508 offsets a N-S striking magnetic-high lineament which extends 80 km southwards into the Permo-
509 Triassic Luangwa Rift in Zambia. We interpret this N-S lineament as a mafic dike that is possibly
510 related to one of the earlier (Triassic or Cretaceous) episodes of rifting which are known to have
511 been associated with extensive late-stage diking events in the Luangwa Rift (e.g., Van de Velde
512 and De Waele, 1998) and Shire Graben in southern Malawi (Castaing, 1991). Sedimentary deposits
513 in the Kaseye-Chitipa area resulted in the burial and lack of sub-aerial exposure of this structure,
514 thus making this study the first revelation of its existence in Northwestern Malawi.

515 Our analyses of the geometry of the interpreted dike structure (Fig. 13A), here in referred
516 to as the Chitipa Dike, shows a distinct difference in the geometry of the structure to the north
517 where it is cut by the strong magnetic-low lineament (continuation of the Ufipa Fault) and to the
518 south (farther away from the fault intersection). South of Chitipa (Fig. 13B), we observe that the
519 north-trending dike describes a consistent left-stepping geometry which diminishes across the
520 Chitipa town location and continues with a more rectilinear geometry northwards into the Mughese
521 Shear Zone area. This side-stepping geometry is typical of vertical sheet intrusions and are related
522 to either magma intrusion into pre-existing stepped joint systems (e.g., Baer, 1991) or near-surface
523 stress rotations during magma intrusion (e.g., Fossen, 2010). In this study, the coincidence and
524 strike of the dike-steps along the NW- to NNW- striking basement fabric may in fact suggest the
525 possible influence of pre-existing basement fabric on the stepping geometries of dike intrusions
526 during their emplacement in host metamorphic rocks (Fig. 13B).

527 Further north, where the dike is cut by the continuation of the Ufipa Fault, the filtered
528 aeromagnetic data shows the dike exhibiting consistent right-lateral offsets across NW-SE

magnetic gradients (Fig. 13C). This clear distinction in the structural style of the dike south of Chitipa and in the north across the continuation of the Ufipa Fault, suggest that the contrasting structural styles are associated with different geological processes. In a summary, we interpret that along the southern boundary of the Mbozi Block, the continuation of the Ufipa Fault, which itself aligns with the Mughese Shear Zone fabric (Fig. 8B-C), is a right-lateral strike-slip fault that displaced a N-S trending Mesozoic (?) dike intrusion (Fig. 13C). We further interpret that this strike-slip fault reactivated the Precambrian Mughese Shear Zone at some time post-Cretaceous (i.e. related to the present Cenozoic rifting phase), and therefore refer to it as the "Mughese Fault". This interpretation is further supported by the change in the morphological expression of the Ufipa Fault from a typical single-scarp style into a narrow linear valley-ridge style in the Tunduma area in the SRTM DEM (see "linear ridge" in Fig. 8A). The observed linear valley-ridge geomorphology is typical of active strike-slip fault zones (e.g., McCalpin et al., 2009). In addition, previous field studies in the area (Delvaux et al., 2012) observed strike-slip displacement on rock outcrops at Tunduma and Mbozi Quarry ("Q" in Fig. 8A). Using the Chitipa Dike as a strain marker, we observe that the offsets increase northwards across multiple splays of the Mughese Fault and estimate that the displacement is maximum at the major Mughese Fault trace (northernmost extent of the strike-slip fault zone). Since mafic intrusions often produce magnetic anomalies larger than the actual size of the sources, it is practically impossible to estimate the true cumulative strike-slip displacement from the aeromagnetic data. Based on the lateral dike separation across the fault on our aeromagnetic data, we estimate a minimum of 500 m lateral displacement along the Mughese Fault (Fig. 13C). It is also possible that this estimated offset only represents the lateral component of an oblique-normal slip along the fault. In Figure 14, we present

551 a conceptual model that summarizes our interpretation of the Chitipa Dike geometry and the
552 interaction of the Mughese Fault with the dike.

553 However, in Tunduma area (Fig. 8A), the presence of discrete breaching of the linear ridge
554 by stream channels suggest that the strike-slip displacement along the Mughese Fault is most-
555 likely a short-lived event that occurred at some time in the past during the development of the
556 RNMRS. The curvilinear fault scarp adjacent to the Mughese Fault at Tunduma shows single-
557 scarp morphology (not linear-ridge morphology) typical of normal faults as seen on the other
558 segments of the Ufipa Fault. Therefore, we interpret this curvilinear fault scarp as a possible old
559 segment of the Ufipa Fault that was 'pirated' by the Mughese strike-slip fault; thus, suggesting a
560 phase in which the Ufipa Fault accommodated strike-slip displacement.

561 Along the southwest margin of the North Malawi Rift (Karonga area), the Mughese Fault
562 diffuses into a zone of wide-spread faulting where the southeast-ward bend of the Mughese Shear
563 Zone controls the development of the normal faults and recent seismicity along the basin hinge
564 margin (Fig. 9A-C) (Kolawole et al., 2018; Dawson et al., 2018). Further south of Karonga town,
565 the NNW-striking Mbiri Fault is the dominant fault structure in terms of its length (and
566 displacement?) along this part of the hinge zone of the North Malawi Rift. We do not observe any
567 direct spatial connectivity between the Mughese Fault and the Mbiri Fault. However, based on the
568 sub-parallel geometry of both faults and the structural dominance of the Mbiri Fault in the area,
569 we suggest that the Mbiri Fault could possibly represent a continuation of the Mughese Fault into
570 the hinge zone of the Malawi Rift North Basin. It is also important to note that the Mbiri Fault is
571 synthetic to the Livingstone border Fault. Following the observations and interpretations above,
572 we suggest that there exists a well-developed continuous connectivity of rift-related structures
573 along the southwestern boundary of the RNMRS, facilitated by the extent of the Mughese Shear

Zone and the Ufipa Terrane. Interestingly, the linking of the oppositely-dipping Ufipa and Mbiri Faults by the Mughese strike-slip fault describes a structure that, overall, is similar to that of the Morley et al. (1990) convergent-approaching normal fault system.

5.3. The Northeastern Boundary of the RNMRS and relationships with Precambrian Basement Fabric

The northern segment of the Lupa Fault exhibits clear alignment with the trend of the Katuma Terrane (Fig. 10) and with a few interpretable magnetic lineaments (likely due to low resolution of the aeromagnetic data). We also note that the Lupa Fault is sub-parallel to the Chisi Suture Zone in this area. Farther south of the Lupa Fault (Kapalala-Kanga area; Figs. 10 A-C), the fault segments occur at a high angle to the Usagaran Belt and Lupa Terrane fabrics, thus indicating an apparent lack of control of pre-existing basement fabric on the propagation of the southern Lupa Fault, except in the coincidence of the fault steps with the trend of the basement fabrics.

The southern segment of the Lupa Fault transitions into the Rungwe Volcanic Province (RVP) where surficial cover of volcanic deposits obscures the southward continuation of the Lupa Fault (Fig. 11A). In addition, the presence of mafic volcanic deposits in the RVP (e.g., Fontijn et al., 2012) makes it difficult to make a reliable interpretation of the magnetic fabric of the underlying Precambrian basement (Fig. 11B). However, we find that a distinct magnetic-high lineament aligns with the Mbaka Fault surface trace (white arrows in Figs. 11A and 11B). Also, the distribution of volcanic centers in the RVP show alignment with both the Mbaka Fault trace and a subtle curvilinear gradient (black arrows in Fig. 11B). Further south, the curvilinear gradient connects with the Livingstone Fault, the northeastern border fault of the North Malawi Rift. This curvilinear gradient coincides with the location and extents of the so-called “Ngozi-Rungwe Line”

of Fontijn et al. (2010), described as a buried fault system that served as a conduit for magmatic fluids to migrate to the surface volcanic vents. Therefore, although it is possible that the magnetic anomalies in this area are affected by remanent magnetization from the volcanic deposits, we interpret that this aeromagnetic gradient provides a possible subsurface evidence of the fault system (Ngozi-Rungwe Line) that connects the Lupa Fault and the Livingstone Fault across the RVP. The filtered aeromagnetic data and previous field studies (e.g., Wheeler and Karson, 1989) shows that the Livingstone Fault segments align with and reactivated the fabric of the Upangwa Terrane (Figs. 11B-C). The observations and interpretations above suggest that there exists a well-developed continuous connectivity of rift-related structures along the northeastern boundary of the RNMRS. However, the relationship between the basement fabric and the buried faults beneath the volcanic deposits remains unclear.

5.4. Implications for Rift Development

5.4.1. Rift Coupling

In the Rukwa Rift, the substantial dominance of the Ufipa Fault rift shoulder over that of the Lupa Fault may imply that the Ufipa Fault is the present-day active border fault of the Rukwa Rift. This proposition may be supported by the hypocentral location of the 1994 Mw5.9 Rukwa earthquake and its aftershoks with epicentral location in the northern part of the rift (Fig. 12; Zhao et al., 1997). The nodal planes of the earthquake focal mechanism solution are broadly consistent with the orientation of both the Lupa and Ufipa faults, and relative position of aftershocks to the main shock is well determined (Fig. 12; Zhao et al., 1997). Considering the uncertainty range of the earthquakes, the spatial distribution of the aftershocks relative to the main shock delineates a sub-horizontal fault zone that most fits the subsurface projection of the Ufipa Fault (Fig. 12). In

addition, field investigations of the Kwera relay ramp (see Fig. 6 for location) revealed features that indicate recent activity along the Ufipa Fault (Delvaux et al., 2012). Camelbeeck and Iranga (1996) observed several lower crustal seismicity in the Rukwa Rift with most of the events clustering beneath the Songwe Trough and the Rungwe Volcanic Province (southern parts of the rift; Fig. 1B). The locations of the clusters suggest activity along the southern Lupa Fault and Mbeya Range Fault. However, since the scarp height (and throw?) of the Ufipa Fault decreases southwards (Fig. 3), and the throw on the Lupa Fault increases southwards (and rapidly along the Songwe Trough) (Morley et al., 1992), we infer that the present border fault role of the Ufipa Fault excludes the southermost parts of the Rukwa Rift.

It has also been observed that the early stage of continental rifting is typically characterized by the development of along-axis alternating polarity of rift segments, rift border faults, uplifted rift flanks (e.g., Bosworth, 1985; Rosendahl, 1987; Hayward and Ebinger, 1996; Lao-Davila et al., 2015). The zones of polarity changes (transfer/accommodation zones) serve to transfer extensional strain between the rift segments and link the border faults which often have variable structural styles and geometries (e.g., Morley et al., 1990; Wilson, 1999). Within young continental rift settings, interactions between these large border faults lead to the systematic coupling of border faults and rift segments across the transfer zones, and subsequent growth of the rift system (e.g., Corti, 2012). Along the RNMRS, the alternating location of the of rift shoulder uplift (SW in Rukwa Rift and NE in North Malawi Rift), typical of coupled rift segments, suggest that the RNMRS can be considered a coupled rift segment. Further, our study here shows that there is in fact, continuous structural continuation along the northeastern and southwestern margins of the RNMRS, typical of a coupled rift segment. Although, studies in the EARS and illustrations of its rift segments had always assumed this to be true, we hereby provide evidence supporting it, for

643 the first time. In the West Antarctic rift system, the localization of recent volcanism along
644 transverse structures within an accommodation zone (the Discovery accommodation zone)
645 suggests active structural interactions between the flanking rift segments (Wilson, 1999).
646 Therefore, we further suggest that the focusing of Neogene volcanism (e.g., Fontijn et al., 2010,
647 2012) along the northeastern boundary faults of the Mbozi accommodation zone (Fig. 15A) may
648 be indicative of the ongoing coupling of the Rukwa and North Malawi Rift's northeastern border
649 faults.
650
651 *5.4.2. Rift Kinematics*
652 Several studies have suggested that the development of the RNMRS has been dominated by dextral
653 strike-slip kinematics (e.g., Chorowicz, 1989; Daly et al., 1989; Wheeler and Karson, 1994;
654 Kervyn et al., 2006; Mortimer et al., 2007). However, analyses of fault architecture, fault-
655 kinematics, paleostress and present-day earthquake focal mechanism solution in the Rukwa Rift
656 show that the present-architecture of the rift largely developed within a pure extensional setting
657 with extension direction orthogonal to the trend of the RNMRS (Morley, 2010; Delvaux et al.,
658 2012). Furthermore, Delvaux et al. (2012) observed dextral strike-slip faulting along the fault
659 systems bounding the Rukwa Rift, but concluded that the strike-slip event was transitory and was
660 associated with an early Mesozoic transpressional event that resulted in the inversion of Karoo
661 sediments. In this study, we observe the existence of a well-defined strike-slip fault bounding the
662 SW margin of the Mbozi Block that reactivated the Precambrian Mughese Shear Zone. We also
663 observe lack of present-day activity along the strike-slip fault, and that this fault displaced a buried
664 mafic dike with at least 500 m of dextral offset.

In the absence of chronological data on the mapped dike, we posit that the dike is most-likely associated with the widespread late-Karoo dike swarms observed in the Luangwa Rift and Shire Graben (southern Malawi) (Castaing, 1991; Van de Velde and De Waele, 1998). We refer to this strike-slip fault as the "Mughese Fault", and the buried dike as the "Chitipa Dike". The Chitipa Dike, presented for the first time in this work, may constitute the most excellent record of strike-slip kinematics along the RNMRS. Although, our results agree with Delvaux et al. (2012) in that the strike-slip faulting along the RNMRS was short-lived, we suggest that future geochronological analyses of this intrusion may provide the most-reliable constraint on the timing of strike-slip faulting event. It is also interesting to note that if the Mughese strike-slip fault is post-Karoo, its development represents a late reactivation of the Mughese Shear Zone in the evolution of the RNMRS. However, late reactivation of rift-oblique basement shear zones is not uncommon in rift basins (e.g., Muirhead and Kattenhorn, 2018).

Following the considerations above, we present cartoons of the RNMRS, illustrating the continuous structural connectivity along the northeast and southwest boundaries guided by the basement fabrics (Fig. 15B), and possible subsurface geometries and interactions of the domain-bounding structures (Fig. 15B-E). The inferred dominance of the Ufipa Fault in the northern and central parts of the Rukwa Rift (Fig. 12) suggest possible truncation of the Lupa Fault at depth, such that the load of the basin hanging wall block is being carried by the Ufipa Fault (Fig. 15B). However, seismic data is needed to confirm this interpretation. We illustrate a possible spatial relationship between the RVP magma pathways and the Mbozi Block bounding faults in Figure 15C. In Figure 15D-E, we show a generalized basin geometry and flip in border fault polarity from the Malawi Rift North Basin to the Usisya Basin. Overall, we posit that, along the northeastern boundary of the Mbozi Block transfer zone strain is accommodated by magmatism utilizing pre-

688 existing fault systems, whereas, along the southwestern boundary, strain is accommodated by
689 dextral strike-slip faulting.
690
691 *5.5. Control of basement fabrics on normal fault geometries*
692 Overall, along the border faults of the Rukwa Rift, we find that strongly-curvilinear normal fault
693 geometries (in plan-view) occur in three distinct settings. One, in areas where the basement fabrics
694 describe high curvatures (>15°) (e.g., in the Chisi area, northern segment of the Lupa Fault; Fig.
695 5). Second, in areas of superposition of discordant sets of basement fabrics, in which the overall
696 fault strike is parallel to one of the sets and relay ramp breach-faults follow the other fabric set that
697 is oblique to the overall fault strike (e.g., central segment of Ufipa Fault; Fig. 6). Third, in areas
698 where the faults propagate at high-angle to the strike of the basement fabrics (e.g., in the Kapalala-
699 Kanga area, southern segment of the Lupa Fault; Fig. 10). In general, along the RNMRS, we find
700 that in areas where the basement fabrics show low curvatures (<10°), the fault segments tend to
701 describe long, rectilinear geometries with narrow or almost unidentifiable breached-relay zones
702 (e.g., Southern Ufipa Fault, Fig. 7; Mughese Fault, Fig. 8; Livingstone Fault, Fig. 11). We suggest
703 that the control of rectilinear (<10° curvature) basement fabrics on the propagation of normal faults
704 may result in the development of rectilinear fault segments with greater likelihood of occurrence
705 of narrow relay ramps and tip-to-tip fault linkage.
706 Curvilinear normal faults have been observed at various scales and at different extensional
707 tectonic settings (Fossen and Rotevatn, 2016). However, the first order curvilinear normal faults
708 are typically characterized by segment boundaries with salients (cusps) that plunge basin-ward
709 e.g., Salt-lake salient and Transverse Mountain salients of the Wasatch Fault in Utah (Fig. 16A),
710 and the Gullfaks salient in the North Sea (Fig. 16B) (Fossen and Rotevatn, 2016). Also, the

711 reported curvilinear faults show characteristic basin-ward concave geometries. However, the
712 South Oquirrh Mountains normal fault zone, although curvilinear (Wu and Bruhn, 1994), exhibits
713 striking basin-ward convex geometry in which the cusps point into the footwall of the fault (Fig.
714 16A). Wu and Bruhn (1994) suggested that convex curvilinear geometry of the South Oquirrh
715 Mountains normal fault zone developed by sequential propagation of the fault into its foot-wall,
716 guided by linkage across smaller en-echelon faults created by the lateral shear components at the
717 tips of the propagating fault. Here, in the Rukwa Rift, we observe both convex- and concave-
718 curvilinear normal fault geometries along the Ufipa and Lupa Faults. The central Ufipa Fault (Fig.
719 6) and southern Lupa Fault (Kapalala-Mwambani area in Fig. 10A-C) exhibit convex-curvilinear
720 normal fault geometries, whereas the northern Ufipa Fault and the Chisi Fault demonstrate
721 concave-curvilinear fault geometries (linked at the Chisi salient) (Fig. 5). Also, we find striking
722 similarities between the concave- and convex-curvilinear fault geometries of the Rukwa Rift (Fig.
723 16C) with those in the southern Malawi Rift (Fig, 16D), the Jurassic sedimentary sequence of the
724 northern North Sea rift (Gullfaks area) (Fig. 16B), and the Provo-Salt Lake City area (Fig. 16A).
725 As show in Figure 16D, the segments of the Bilila-Mtakataka Fault in southern Malawi Rift present
726 excellent examples of convex-curvilinear normal fault geometries (Jackson and Blekinsop, 1997).
727 Recent studies on the relationships between the basement fabrics and the Bilila-Mtakataka Fault
728 segments (Johnson et al., 2018; Hodge et al., 2018) show that some of the segments appear to align
729 with the distributed basement fabrics, while others cut across the basement fabrics.

730 Based on the observations above, we present conceptual models for the control of various
731 configurations of pre-existing basement fabrics on the development of curvilinear normal fault
732 plan-view geometries (Fig. 17). We show how discrete and distributed basement fabrics and
733 combinations of the two categories of fabrics can influence the plan-view geometry of normal

faults. However, there is need to better understand (1) the influence of the basement fabrics on the geometries of curvilinear normal faults in 3-dimensions, (2) the influence of the extension direction on the development of the observed curvilinear normal faults in areas where the basement fabric present mechanical anisotropy.

Although, Fossen and Rotevatn (2016) provide evidence of subsidiary short-cut faulting across a salient, suggesting an impending evolution of concave-curvilinear faults into rectilinear faults, it is not yet clear if the model applies to convex-curvilinear normal faults since the two styles of faults are geometrically different. However, the synthetic Bilila-Mtakataka and the Chirobwe-Ncheu Faults (Fig. 16D) in southern Malawi Rift may provide some insight. Since the Chirobwe-Ncheu Fault is older than the Bilila-Mtakataka Fault (Jackson and Blekinsop, 1997), the rectilinear geometry of the Chirobwe-Ncheu Fault suggests that the apices of convex curvilinear segments may likewise eventually get breached to form more-rectilinear fault segments. Conversely, we observe the opposite of this model along the Lupa Fault, where the more-rectilinear northern Lupa Fault has accommodated much less strain compared to its curvilinear southern segment which has the most strain within the Rukwa Rift (Morley et al., 1992). Therefore, we suggest that although the model of temporal progression from a curvilinear to rectilinear fault geometry may apply to some large normal faults, it may not apply to others.

5.6. Rift Bifurcation

The basin scale splaying of the Rukwa Rift around the Mbozi Block into the Musangano and Songwe Troughs (Fig. 1B) obviously represents a smaller-scale of rift bifurcation when compared to the continental scale bifurcation of rift systems around microplates. Examples of such continental-scale rift bifurcation include the branching of the East African Rift around the

Tanzania microplate into the western and eastern branches (Fig. 1A; e.g., Rosendahl, B.R., 1987; Versfelt and Rosendahl, 1989), the Red Sea Rift around the Sinai microplate into the Gulf of Suez Rift and Dead Sea Transform, and the South Atlantic Rift around the Sergipe microplate into the Tucano-Recôncavo Rift and Sergipe-Alagoas Transform (e.g., Szatmari and Milani, 1999) (Figs. 18A-C). Based on scale distinction, we therefore refer to the continental rift-system scale bifurcation as first (1^{st}) order rift bifurcation (Figs. 18A-C) and the rift-basin scale bifurcation as second (2^{nd}) order rift bifurcation (Fig. 18D-F). Similar to the Rukwa Rift, 2^{nd} order rift bifurcations are common along the East African Rift System. Examples include the Southern Malawi Rift bifurcation around the Shire Horst, the Shire Graben bifurcation around the Namalambo Horst, and the Albertine Graben bifurcation around the Rwenzori Block (Fig. 18B; e.g., Castaing, 1991; Koehn et al., 2008; Lao-Davila et al., 2015; Xue et al., 2017).

Regardless of scale, numerical models have showed that inherited structural heterogeneity and lateral strength variations are key controls on rift bifurcation (e.g., Brune and Autin, 2013; Brune et al., 2017). However, it appears that 1^{st} order bifurcations commonly occur at the tip of pre-existing microcratonic blocks along the path of propagation of a continental rift system (e.g., Fig. 18A). Also, 2^{nd} order bifurcations appear to occur at the transfer zones between approaching rift segments, possibly due to a high tendency for the development of interfingering fault blocks in the transfer zones between colinear approaching rift segments (Morley, 1995) and lateral rotation of the trapped blocks in the transfer zones between overlapping approaching rift segments (Koehn et al., 2008).

It is possible that the bifurcation of the Rukwa Rift around the Mbozi Block is related to the location of the block within the transfer zone of the colinear approaching Rukwa and North Malawi Rift segments. However, we suggest that the basement fabrics of the Ubendian Belt around

780 the Mbozi Block transfer zone could be playing a complementary role in facilitating and guiding
781 the intra-rift bifurcation of the Rukwa Rift around the block. Our filtered aeromagnetic map (Fig.
782 4B) shows that the block is dominated by a WNW-ESE and N-S fabrics. According to Daly (1988),
783 the Meta-basites and intermediate granulites and quartzites of the Mbozi Block are characterized
784 by lineations that trend NE-SW. These observations, however, suggest that the Mbozi Block
785 fabrics strike at oblique to high-angles to the trend of the colinear fabrics of the basement terranes
786 bounding the Mbozi Block (Katuma-Upangwa Terranes to the northeast, and those of the Ufipa
787 Terrane to the southwest) and the main rift-bounding faults (the Lupa, Ufipa, Livingstone and
788 Mughese Faults) (Fig. 15A). Therefore, we suggest that the colinear fabrics of the basement
789 terranes surrounding the Mbozi Block which are already controlling the propagation and linking
790 of the rift-bounding faults may be playing a significant role in guiding the bifurcation of the Rukwa
791 Rift around the Mbozi Block (Figs. 4B, 7, 8 and 11).
792
793 **6.0 CONCLUSIONS**
794 Our topographic analyses of the morphology of the RNMRS and detailed study of the
795 relationships between the pre-existing basement fabric and rift-related faults provide, for the first
796 time, evidence supporting the coupling of the Rukwa and North Malawi Rift. Our topographic
797 analyses in the Rukwa Rift suggest that the Ufipa Fault is the present-day active border fault of
798 the rift. We find that the Ufipa fault is the dominant topographic feature in the northern part of the
799 RMNRS and diminishes as it encounters the Mbozi block where it becomes a strike slip fault
800 (Mughese Fault), at which point the border fault polarity flips and the Livingstone Fault is the
801 dominant fault in the southern part of the RNMRS.

Further, we demonstrate the continuity structures along the northeastern and southwestern margins of the RNMRS. We show that this structural connectivity across the Mbozi Block transfer zone between the rifts is guided by the pre-existing Precambrian terrane fabrics and associated shear zones. We show that the coupling of the RNMRS along the northeastern boundary of the Mbozi Block transfer zone is accommodated by magmatism along the linking faults, whereas, coupling along the southwestern boundary is accommodated by strike-slip faulting. Overall, we suggest that the continuation of the boundary faults along the RNMRS, and their alignment with colinear Precambrian basement fabric and shear zones indicate the influence of the pre-existing basement structures on the coupling and amalgamation of approaching colinear rift segments. On the basin-scale bifurcation of the Rukwa Rift, we infer that the discordance of the basement fabrics within the Mbozi Block transfer zone to those of the basement terranes bounding it may have facilitated the development of intra-rift bifurcation of the rift around the transfer zone.

Furthermore, we show the influence of pre-existing basement fabrics on the development of the RNMRS as evidenced in the geometry, termination and kinematics of the rift-bounding fault segments. Our observations suggest that curvilinear normal fault geometries developed in areas where the basement fabrics are either curvilinear, composed of superposed sets of differently-orientated fabrics, or not favorably oriented to the extensional stress field. Whereas, long, rectilinear fault geometries with narrow or almost unidentifiable breached-relay zones developed in areas where the pre-existing basement fabrics are roughly rectilinear, suggesting the greater likelihood of occurrence of tip-to-tip linkage of fault segments.

Finally, we present the existence of a buried Pre-Cenozoic strike-slip-faulted mafic dike, which we suggest is potentially the most excellent record of strike-slip kinematics along the RNMRS. We further suggest that future geochronological analyses of this intrusion may provide

825 the most-reliable constraint on the timing of the controversial strike-slip faulting event along the
826 RNMRS.
827
828 **Acknowledgements**
829 This work was partially supported by the National Science Foundation (NSF) grant EAR10-09988
830 (awarded to E.A. Atekwana). Also, we acknowledge the Oklahoma State University (OSU) for the
831 Niblack Scholarship awarded to Erin Heilman. We thank the Geological Survey Department of
832 Malawi for allowing us to purchase the 2013 aeromagnetic data used in this study. We also thank
833 the Zambia Geological Survey for allowing us to purchase the aeromagnetic data used in this study.
834 We thank South African Development Community (SADC) for providing the Tanzania
835 aeromagnetic data used in this study. This is the Oklahoma State University Boone Pickens School
836 of Geology contribution no. 2018-.
837
838
839 **References**
840 Baer, G., 1991. Mechanisms of dike propagation in layered rocks and in massive, porous
841 sedimentary rocks. *Journal of Geophysical Research: Solid Earth*, *96*(B7), pp.11911-
842 11929.
843 Baranov, V., 1957. A new method for interpretation of aeromagnetic maps: pseudo-gravimetric
844 anomalies. *Geophysics*, *22*(2), pp.359-382.
845 Boniface, N. and Schenk, V., 2012. Neoproterozoic eclogites in the Paleoproterozoic Ubendian
846 belt of Tanzania: Evidence for a Pan-African suture between the Bangweulu block and
847 the Tanzania craton. *Precambrian Research*, *208*, pp.72-89.

Boniface, N., Schenk, V. and Appel, P., 2012. Paleoproterozoic eclogites of MORB-type chemistry and three Proterozoic orogenic cycles in the Ubendian Belt (Tanzania): Evidence from monazite and zircon geochronology, and geochemistry. *Precambrian Research*, *192*, pp.16-33.

Borrego, D.J., 2016. Crustal Structure of the Rungwe Volcanic Province and Region Surrounding the Northern Lake Malawi Rift Basin. MSc Thesis, Pennsylvania State University.

Bosworth, W., 1985. Geometry of propagating continental rifts. *Nature*, *316*(6029), p.625.

Boven, A., Theunissen, K., Sklyarov, E., Klerkx, J., Melnikov, A., Mruma, A. and Punzalan, L., 1999. Timing of exhumation of a high-pressure mafic granulite terrane of the Paleoproterozoic Ubende belt (West Tanzania). *Precambrian Research*, *93*(1), pp.119-137.

Brune, S. and Autin, J., 2013. The rift to break-up evolution of the Gulf of Aden: Insights from 3D numerical lithospheric-scale modelling. *Tectonophysics*, *607*, pp.65-79.

Brune, S., Corti, G. and Ranalli, G., 2017. Controls of inherited lithospheric heterogeneity on rift linkage: Numerical and analog models of interaction between the Kenyan and Ethiopian rifts across the Turkana depression. *Tectonics*, *36*(9), pp.1767-1786.

Camelbeeck, T. and Iranga, M.D., 1996. Deep crustal earthquakes and active faults along the Rukwa trough, eastern Africa. *Geophysical Journal International*, *124*(2), pp.612-630.

Castaing, C., 1991. Post-Pan-African tectonic evolution of South Malawi in relation to the Karroo and recent East African rift systems. *Tectonophysics*, *191*(1-2), pp.55-73.

869 Chorowicz, J., 1989. Transfer and transform fault zones in continental rifts: examples in the
870 Afro-Arabian rift system. Implications of crust breaking. *Journal of African Earth*
871 *Sciences (and the Middle East), 8(2-4)*, pp.203-214.
872 Chorowicz, J., 2005. The east African rift system. *Journal of African Earth Sciences*, *43*(1),
873 pp.379-410.
874 Collanega, L., Bell, R., Coleman, A.J., Lenhart, A. and Breda, A., 2018. How do intra-basement
875 fabrics influence normal fault growth? Insights from the Taranaki Basin, offshore New
876 Zealand. EarthArxiv, DOI: 10.31223/osf.io/8rn9u
877 Corti, G., 2012. Evolution and characteristics of continental rifting: Analog modeling-inspired
878 view and comparison with examples from the East African Rift System. *Tectonophysics*,
879 *522*, pp.1-33.
880 Daly, M.C., 1988. Crustal Shear Zones in Central Africa - A kinematic approach to Proterozoic
881 Tectonics. *Episodes*, *11*(1), pp.5-11.
882 Daly, M.C., Chorowicz, J. and Fairhead, J.D., 1989. Rift basin evolution in Africa: the influence
883 of reactivated steep basement shear zones. *Geological Society, London, Special*
884 *Publications*, *44*(1), pp.309-334.
885 Dawson, S.M., Laó-Dávila, D.A., Atekwana, E.A. and Abdelsalam, M.G., 2018. The influence
886 of the Precambrian Mughese Shear Zone structures on strain accommodation in the
887 northern Malawi Rift. *Tectonophysics*, *722*, pp.53-68.
888 Delvaux, D., and Hanon, M., 1991. Neotectonics of the Mbeya area, SW Tanzania. *Annual*
889 *report of the Royal Museum of Central Africa, Department of Geology and*
890 *Mineralogy*, *1992*, pp.87-97.

Delvaux, D., Kervyn, F., Macheyeki, A.S. and Temu, E.B., 2012. Geodynamic significance of the TRM segment in the East African Rift (W-Tanzania): Active tectonics and paleostress in the Ufipa plateau and Rukwa basin. *Journal of Structural Geology*, *37*, pp.161-180.

Delvaux, D., Levi, K., Kajara, R. and Sarota, J., 1992. Cenozoic paleostress and kinematic evolution of the Rukwa–North Malawi rift valley (East African Rift System). *Bulletin des Centres de Recherche Exploration-Production ElfAquitaine*, *16*, pp.383-406.

Fernandez-Alonso, M., Delvaux, D., Klerkx, J. and Theunissen, K., 2001. Structural link between Tanganyika-and Rukwa-rift basins at Karema-Nkamba (Tanzania): basement structural control and recent evolution. *Mus. Roy. Afr. Centr., Tervuren (Belgique), Dép. Géol. Min., Rap. Ann*, pp.91-100.

Fontijn, K., Delvaux, D., Ernst, G.G., Kervyn, M., Mbede, E. and Jacobs, P., 2010. Tectonic control over active volcanism at a range of scales: case of the Rungwe Volcanic Province, SW Tanzania; and hazard implications. *Journal of African Earth Sciences*, *58*(5), pp.764-777.

Fontijn, K., Williamson, D., Mbede, E. and Ernst, G.G., 2012. The Rungwe Volcanic Province, Tanzania–A volcanological review. *Journal of African Earth Sciences*, *63*, pp.12-31.

Fossen, H., 2010. *Structural geology*. Cambridge University Press.

Fossen, H. and Rotevatn, A., 2016. Fault linkage and relay structures in extensional settings—A review. *Earth-Science Reviews*, *154*, pp.14-28.

Foster, A., Ebinger, C., Mbede, E. and Rex, D., 1997. Tectonic development of the northern Tanzanian sector of the East African Rift System. *Journal of the Geological Society*, *154*(4), pp.689-700.

913 Fritz, H., Abdelsalam, M., Ali, K.A., Bingen, B., Collins, A.S., Fowler, A.R., Ghebreab, W.,
914 Hauzenberger, C.A., Johnson, P.R., Kusky, T.M. and Macey, P., 2013. Orogen styles in
915 the East African Orogen: a review of the Neoproterozoic to Cambrian tectonic
916 evolution. *Journal of African Earth Sciences*, *86*, pp.65-106.
917 Gawthorpe, R.L., Jackson, C.A.L., Young, M.J., Sharp, I.R., Moustafa, A.R. and Leppard, C.W.,
918 2003. Normal fault growth, displacement localisation and the evolution of normal fault
919 populations: the Hammam Faraun fault block, Suez rift, Egypt. *Journal of Structural*
920 *Geology*, *25*(6), 883-895.
921 Grauch, V.J.S. and Hudson, M.R., 2007. Guides to understanding the aeromagnetic expression of
922 faults in sedimentary basins: Lessons learned from the central Rio Grande rift, New
923 Mexico. *Geosphere*, *3*(6), pp.596-623.
924 Grauch, V.J.S. and Hudson, M.R., 2011. Aeromagnetic anomalies over faulted strata. *The*
925 *Leading Edge*, *30*(11), pp.1242-1252.
926 Gudmundsson, A. and Brenner, S.L., 2001. How hydrofractures become arrested. *Terra*
927 *Nova*, *13*(6), pp.456-462.
928 Hayward, N.J. and Ebinger, C.J., 1996. Variations in the along-axis segmentation of the Afar
929 Rift system. *Tectonics*, *15*(2), pp.244-257.
930 Helgeson, D.E. and Aydin, A., 1991. Characteristics of joint propagation across layer interfaces
931 in sedimentary rocks. *Journal of Structural Geology*, *13*(8), pp.897-911.
932 Henderson, R.G. and Zietz, I., 1949. The upward continuation of anomalies in total magnetic
933 intensity fields. *Geophysics*, *14*(4), pp. 517-534.

934 Hodge, M., Fagereng, Å., Biggs, J., and Mdala, H., 2018.. Controls on early-rift geometry: New
935 perspectives from the Bilila-Mtakataka fault, Malawi. *Geophysical Research Letters, 45*,
936 3896–3905.
937 Hodgson, I., Illsley-Kemp, F., Gallacher, R.J., Keir, D., Ebinger, C.J. and Mtelela, K., 2017.
938 Crustal structure at a young continental rift: A receiver function study from the
939 Tanganyika Rift. *Tectonics*, *36*(12), pp.2806-2822.
940 Jackson, J. and Blenkinsop, T., 1997. The Bilila-Mtakataka fault in Malaŵi: An active, 100-km
941 long, normal fault segment in thick seismogenic crust. *Tectonics*, *16*(1), pp.137-150.
942 Johnson, S., Mendez, K., Beresh, S.C.M., Mynatt, W.G., Elifritz, E.A., Laó-Dávila, D.A.,
943 Atekwana, E.A., Abdelsalam, M.G., Chindandali, P.R.N., Chisenga, C. and Gondwe, S.,
944 2017.. The Relationships of Subparallel Synthetic Faults and Pre-existing Structures in
945 the Central Malawi Rift. *AGU Fall Meeting poster number T22C-03*.
946 Katumwehe, A.B., Abdelsalam, M.G. and Atekwana, E.A., 2015. The role of pre-existing
947 Precambrian structures in rift evolution: The Albertine and Rhino grabens,
948 Uganda. *Tectonophysics*, *646*, pp.117-129.
949 Kervyn, F., Ayub, S., Kajara, R., Kanza, E. and Temu, B., 2006. Evidence of recent faulting in
950 the Rukwa rift (West Tanzania) based on radar interferometric DEMs. *Journal of African*
951 *Earth Sciences*, *44*(2), pp.151-168.
952 Kilembe, E.A. and Rosendahl, B.R., 1992. Structure and stratigraphy of the Rukwa
953 rift. *Tectonophysics*, *209*(1-4), pp.143-158.
954 Kim, S., Nyblade, A.A. and Baag, C.E., 2009. Crustal velocity structure of the Rukwa Rift in the
955 western branch of the East African Rift system. *South African Journal of Geology*, *112*(3-
956 4), pp.251-260.

957 Kinabo, B.D., Atekwana, E.A., Hogan, J.P., Modisi, M.P., Wheaton, D.D. and Kampunzu, A.B.,
958 2007. Early structural development of the Okavango rift zone, NW Botswana. *Journal of*
959 *African Earth Sciences*, *48*(2), pp.125-136.
960 Kinabo, B.D., Hogan, J.P., Atekwana, E.A., Abdelsalam, M.G. and Modisi, M.P., 2008. Fault
961 growth and propagation during incipient continental rifting: Insights from a combined
962 aeromagnetic and Shuttle Radar Topography Mission digital elevation model
963 investigation of the Okavango Rift Zone, northwest Botswana. *Tectonics*, *27*(3).
964 Koehn, D., Aanyu, K., Haines, S. and Sachau, T., 2008. Rift nucleation, rift propagation and the
965 creation of basement micro-plates within active rifts. *Tectonophysics*, *458*(1-4), pp.105-
966 116.
967 Kolawole, F., Atekwana, E.A., Laó-Dávila, D.A., Abdelsalam, M.G., Chindandali, P.R., Salima,
968 J. and Kalindekafe, L., 2018. Active deformation of Malawi Rift's North Basin hinge
969 zone modulated by reactivation of pre-existing Precambrian shear zone fabric. *Tectonics*,
970 *37*, pp.683–704.
971 Lao-Davila, D.A., Al-Salmi, H.S., Abdelsalam, M.G. and Atekwana, E.A., 2015. Hierarchical
972 segmentation of the Malawi Rift: The influence of inherited lithospheric heterogeneity
973 and kinematics in the evolution of continental rifts. *Tectonics*, *34*(12), pp.2399-2417.
974 Lawley, C.J., Selby, D., Condon, D.J., Horstwood, M., Millar, I., Crowley, Q. and Imber, J.,
975 2013. Lithogeochemistry, geochronology and geodynamic setting of the Lupa Terrane,
976 Tanzania: implications for the extent of the Archean Tanzanian Craton. *Precambrian*
977 *Research*, *231*, pp.174-193.

978 Lenoir, J.L., Liégeois, J.P., Theunissen, K. and Klerkx, J., 1994. The Palaeoproterozoic
979 Ubendian shear belt in Tanzania: geochronology and structure. *Journal of African Earth*
980 *Sciences, 19*(3), pp.169-184.
981 Mbede, E.I., 2002. Interpretation of refelction seismic data from the Usangu Basin, East African
982 Rift System. *Tanzania Journal of Science, 28*(1), pp.83-97.
983 McCalpin, J.P., Rockwell, T.K. and Weldon II, R.J., 2009. Paleoseismology of Strike-Slip
984 Tectonic Environments. *International Geophysics, 95*, pp.421-496.
985 Modisi, M.P., Atekwana, E.A., Kampunzu, A.B. and Ngwisanyi, T.H., 2000. Rift kinematics
986 during the incipient stages of continental extension: Evidence from the nascent Okavango
987 rift basin, northwest Botswana. *Geology, 28*(10), pp.939-942.
988 Morley, C.K., 1995. Developments in the structural geology of rifts over the last decade and their
989 impact on hydrocarbon exploration. *Geological Society, London, Special*
990 *Publications*, *80*(1), pp.1-32.
991 Morley, C.K., 2010. Stress re-orientation along zones of weak fabrics in rifts: An explanation
992 for pure extension in 'oblique' rift segments?. *Earth and Planetary Science*
993 *Letters*, *297*(3), pp.667-673.
994 Morley, C.K., Cunningham, S.M., Harper, R.M. and Wescott, W.A., 1992. Geology and
995 geophysics of the Rukwa rift, East Africa. *Tectonics, 11*(1), pp.69-81.
996 Morley, C.K., Nelson, R.A., Patton, T.L. and Munn, S.G., 1990. Transfer zones in the East
997 African rift system and their relevance to hydrocarbon exploration in rifts (1). *AAPG*
998 *Bulletin, 74*(8), pp.1234-1253.

Mortimer, E., Paton, D.A., Scholz, C.A., Strecker, M.R. and Blisniuk, P., 2007. Orthogonal to oblique rifting: effect of rift basin orientation in the evolution of the North basin, Malawi Rift, East Africa. *Basin Research*, *19*(3), pp.393-407.

Muirhead, J.D. and Kattenhorn, S.A., 2018. Activation of preexisting transverse structures in an evolving magmatic rift in East Africa. *Journal of Structural Geology*, *106*, pp.1-18.

Njinju, E.A., Atekwana, E.A., Stamps, D.S., Abdelsalam, M.G., Atekwana, E.A., Mickus, K.L., Kolawole, F. and Nyalugwe, V., 2018. Lithospheric Structure of the Malawi Rift: Implications for Rifting Processes in Magma Poor Rift Systems. *EarthArXiv*, DOI: 10.31223/osf.io/83qd9

Peirce, J.W. and Lipkov, L., 1988. Structural interpretation of the Rukwa rift, Tanzania. *Geophysics*, *53*(6), pp.824-836.

Phillips, T.B., Jackson, C.A., Bell, R.E., Duffy, O.B. and Fossen, H., 2016. Reactivation of intrabasement structures during rifting: A case study from offshore southern Norway. *Journal of Structural Geology*, *91*, pp.54-73.

Pik, R., Marty, B., Carignan, J., Yirgu, G. and Ayalew, T., 2008. Timing of East African Rift development in southern Ethiopia: Implication for mantle plume activity and evolution of topography. *Geology*, *36*(2), pp.167-170.

Ring, U., Kröner, A., Buchwaldt, R., Toulkeridis, T. and Layer, P.W., 2002. Shear-zone patterns and eclogite-facies metamorphism in the Mozambique belt of northern Malawi, east-central Africa: implications for the assembly of Gondwana. *Precambrian Research*, *116*(1), pp.19-56.

Rosendahl, B.R., 1987. Architecture of continental rifts with special reference to East Africa. *Annual Review of Earth and Planetary Sciences*, *15*(1), pp.445-503.

1022 Rotevatn, A., Jackson, C.A.L., Tvedt, A.B.M., Bell, R. and Blækkan, I., 2018. How do normal
1023 faults grow?. EarthArXiv.
1024 Salem, A., Williams, S., Fairhead, J.D., Ravat, D. and Smith, R., 2007. Tilt-depth method: A
1025 simple depth estimation method using first-order magnetic derivatives. *The Leading*
1026 *Edge*, *26*(12), pp.1502-1505.
1027 Sarafian, E., Evans, R.L., Abdelsalam, M.G., Atekwana, E., Elsenbeck, J., Jones, A.G. and
1028 Chikambwe, E., 2018. Imaging Precambrian lithospheric structure in Zambia using
1029 electromagnetic methods. *Gondwana Research*, *54*, pp.38-49.
1030 Scholz, C.H. and Contreras, J.C., 1998. Mechanics of continental rift architecture. *Geology*,
1031 *26*(11), pp.967-970.
1032 Silva, J.B., 1986. Reduction to the pole as an inverse problem and its application to low-latitude
1033 anomalies. *Geophysics*, *51*(2), pp.369-382.
1034 Siuda, K., Magee, C., Bell, R., Jackson, C.A.L. and Collanega, L., 2018. Pre-existing basement
1035 thrusts influence rifting in the Taranaki Basin, New Zealand. EarthArXiv.
1036 Szatmari, P. and Milani, E.J., 1999. Microplate rotation in northeast Brazil during South Atlantic
1037 rifting: Analogies with the Sinai microplate. *Geology*, *27*(12), pp.1115-1118.
1038 Taylor, B., Weiss, J.R., Goodliffe, A.M., Sachpazi, M., Laigle, M. and Hirn, A., 2011. The
1039 structures, stratigraphy and evolution of the Gulf of Corinth rift, Greece. *Geophysical*
1040 *Journal International*, *185*(3), pp.1189-1219.
1041 Theunissen, K., Klerkx, J., Melnikov, A. and Mruma, A., 1996. Mechanisms of inheritance of
1042 rift faulting in the western branch of the East African Rift, Tanzania. *Tectonics*, *15*(4),
1043 pp.776-790.

1044 Van de Velde, P., and De Waele, B., 1998. Geology of the Mupamadzi River area. Explanation
1045 of degree sheet 1231, SW quarter, Report No. 105, *Geological Survey Department,*
1046 *Republic of Zambia.*
1047 Versfelt, J. and Rosendahl, B.R., 1989. Relationships between pre-rift structure and rift
1048 architecture in Lakes Tanganyika and Malawi, East Africa. *Nature, 337*(6205), p.354.
1049 Wheeler, W.H. and Karson, J.A., 1989. Structure and kinematics of the Livingstone Mountains
1050 border fault zone, Nyasa (Malawi) Rift, southwestern Tanzania. *Journal of African Earth*
1051 *Sciences (and the Middle East), 8*(2-4), pp.393-413.
1052 Wheeler, W.H. and Karson, J.A., 1994. Extension and subsidence adjacent to a "weak"
1053 continental transform: An example from the Rukwa rift, East Africa. *Geology*, *22*(7),
1054 pp.625-628.
1055 Wichura, H., Bousquet, R., Oberhänsli, R., Strecker, M.R. and Trauth, M.H., 2011. The Mid-
1056 Miocene East African Plateau: a pre-rift topographic model inferred from the
1057 emplacement of the phonolitic Yatta lava flow, Kenya. *Geological Society, London,*
1058 *Special Publications, 357*(1), pp.285-300.
1059 Wilson, T.J., 1999. Cenozoic structural segmentation of the Transantarctic Mountains rift flank
1060 in southern Victoria Land. *Global and Planetary Change*, *23*(1-4), pp.105-127.
1061 Wu, D. and Bruhn, R.L., 1994. Geometry and kinematics of active normal faults, South Oquirrh
1062 Mountains, Utah: implication for fault growth. *Journal of Structural Geology*, *16*(8),
1063 pp.1061-1075.
1064 Xue, L., Gani, N.D. and Abdelsalam, M.G., 2017. Geomorphologic proxies for bedrock rivers:
1065 A case study from the Rwenzori Mountains, East African Rift system. *Geomorphology*,
1066 *285*, pp.374-398.

Zhang, X. and Jeffrey, R.G., 2008. Reinitiation or termination of fluid-driven fractures at frictional bedding interfaces. *Journal of Geophysical Research: Solid Earth*, *113*(B8).

Zhang, X., Jeffrey, R.G. and Thiercelin, M., 2007. Deflection and propagation of fluid-driven fractures at frictional bedding interfaces: a numerical investigation. *Journal of Structural Geology*, *29*(3), pp.396-410.

Zhao, M., Langston, C.A., Nyblade, A.A. and Owens, T.J., 1997. Lower-crustal rifting in the Rukwa graben, East Africa. *Geophysical Journal International*, *129*(2), pp.412-420.

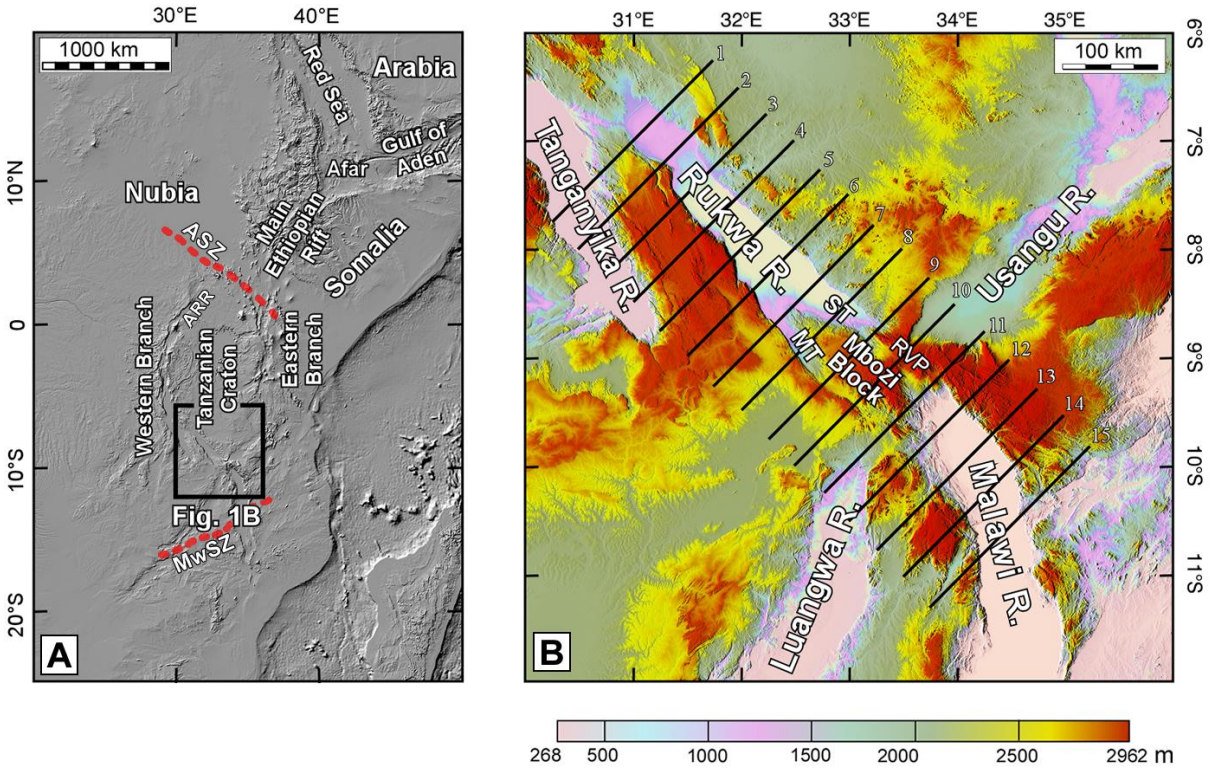

Fig.1. (A) Topographic map of the East African Rift System, showing the segments of the rift system and the location of the Rukwa-North Malawi Rift Segment (RNMRS) (black square). (B) Digital Elevation Model (DEM) of the RNMRS showing the different domains. Solid black lines represent topographic profile lines shown in Figure 3. ARR= Albertine-Rhino Rift, ASZ= Aswa Shear Zone, MT= Musangano Trough, MwSZ= Mwembeshi Shear Zone, RVP= Rungwe Volcanic Province, ST= Songwe Trough.

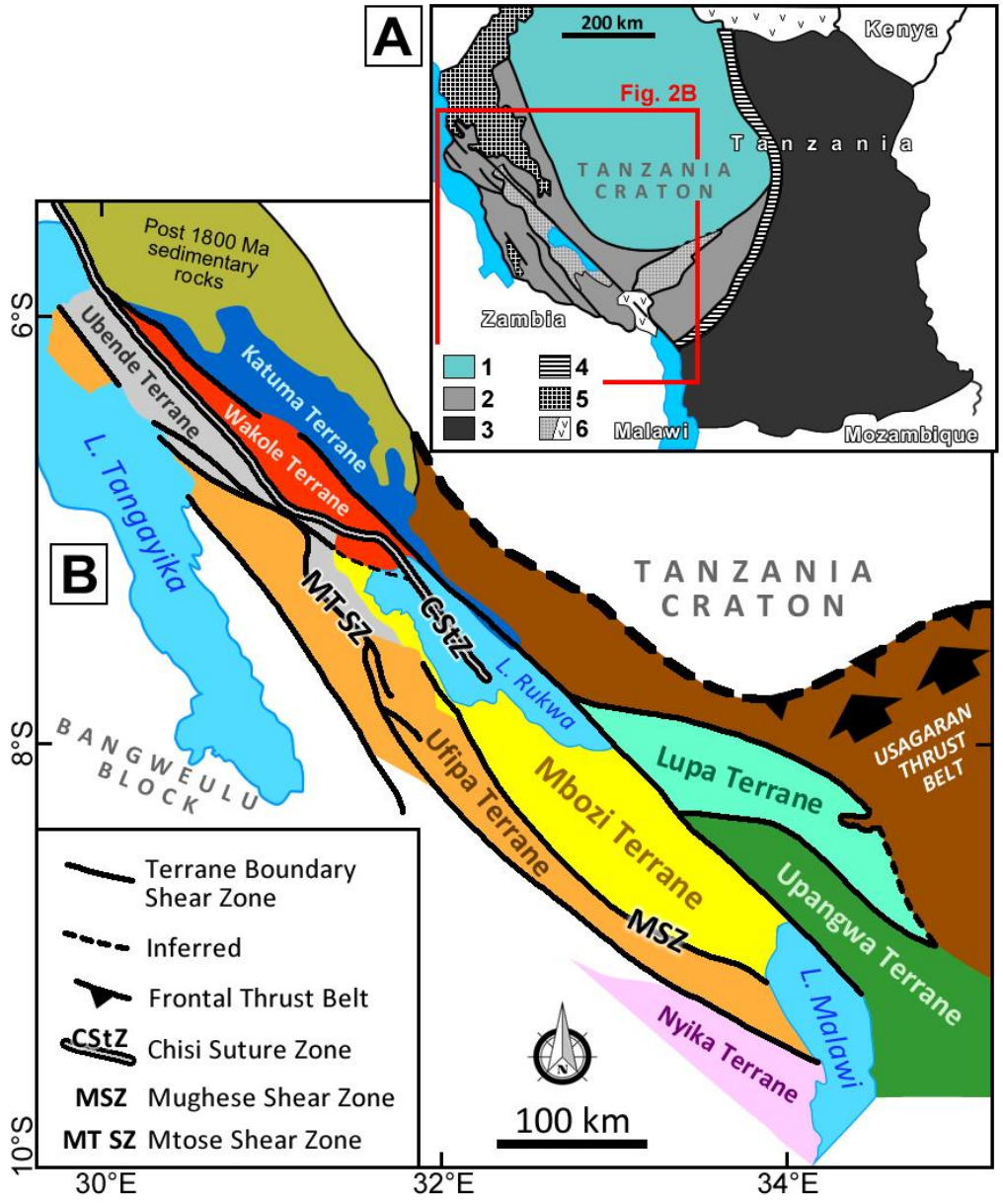

Fig. 2. (A) Precambrian domains around the Tanzanian Craton (modified after Theunissen et al., 1996; Boven et al., 1999; Fernandez-Alonso et al., 2001; Boniface and Schenk, 2012; Delvaux et al., 2012). 1 = Archean craton; 2 = Paleoproterozoic Usagaran and Ubendian orogenic belts; 3 = Mozambique orogenic belt; 4 = western limit of Pan-African influence; 5 = Meso and/or Neoproterozoic sediments *(only for the Ubendian Belt region)*; 6 = Phanerozoic volcanics and sedimentary rocks. (B) Regional geological map of southwest Tanzania showing the terrane structure of the Ubendian orogenic belt within which the Rukwa-Malawi Rift Segment (RNMRS) developed.

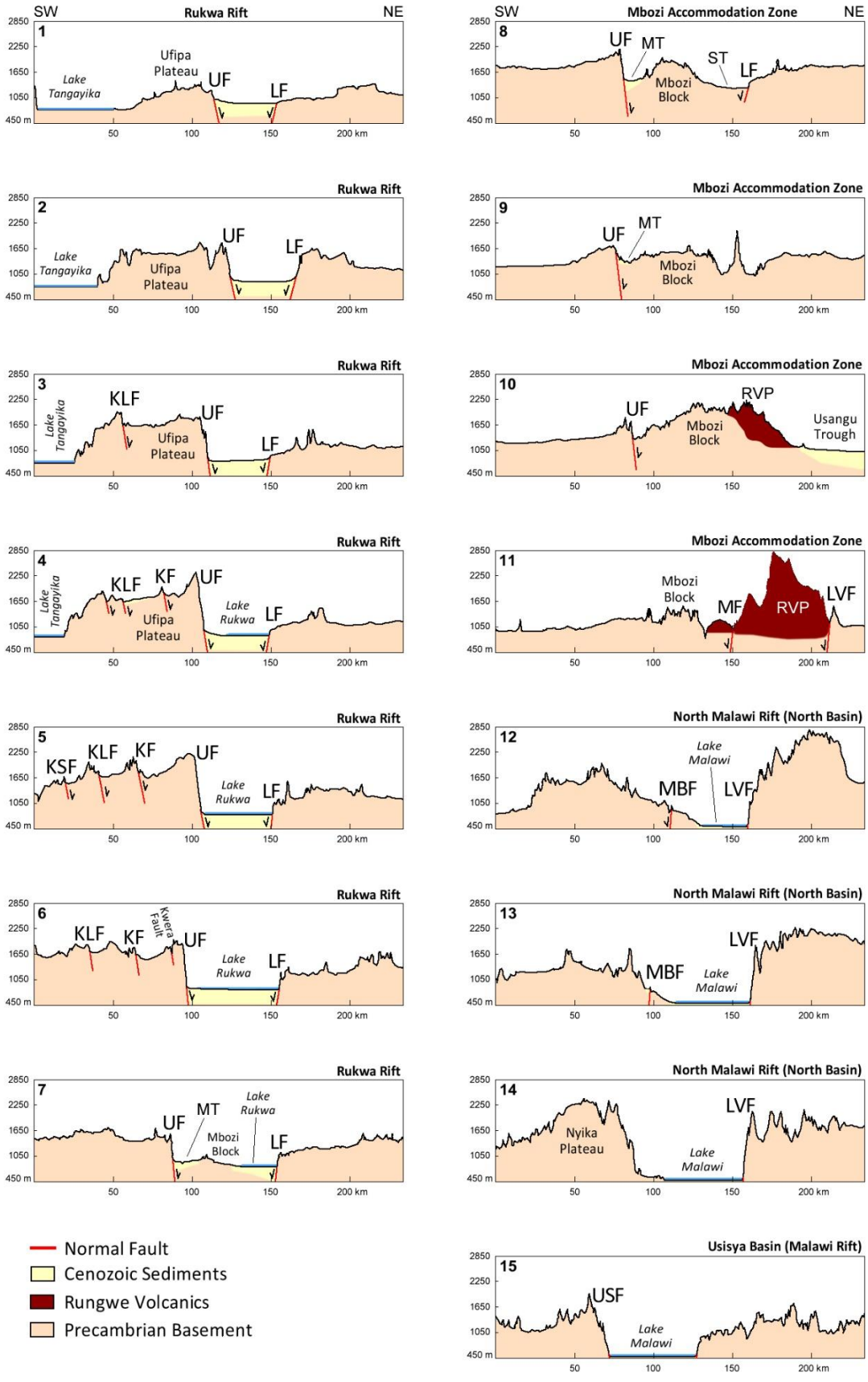
SW
Rukwa Rift
NE
1
Lake Tangayika
Ufipa Plateau
UF
LF
2
KLF
3
KF
4
Lake Rukwa
5
KSF
6
Kwera Fault
7
MT
Mbozi Block
Mbozi Accommodation Zone
8
ST
9
10
RVP
Usangu Trough
11
MF
LVF
North Malawi Rift (North Basin)
12
Lake Malawi
MBF
13
14
Nyika Plateau
Usisya Basin (Malawi Rift)
15
USF
2850
2250
1650
1050
450 m
50
100
150
200 km
Normal Fault
Cenozoic Sediments
Rungwe Volcanics
Precambrian Basement

Fig. 3. Topographic profiles across the Rukwa - North Malawi Rift segment. Profile numbers correspond to the profiles in Figure 1B. KLF = Kalambo Fault, KF = Kanda Fault, KSF = Kasanga Fault, LF = Lupa Fault, LVF = Livingstone Fault, MB = Mbozi Block, MBF = Mbiri Fault, MF = Mbaka Fault, MT = Musangano Trough, RVP = Rungwe Volcanic Province, ST = Songwe Trough, UF = Ufipa Fault, USF = Usisya Fault.

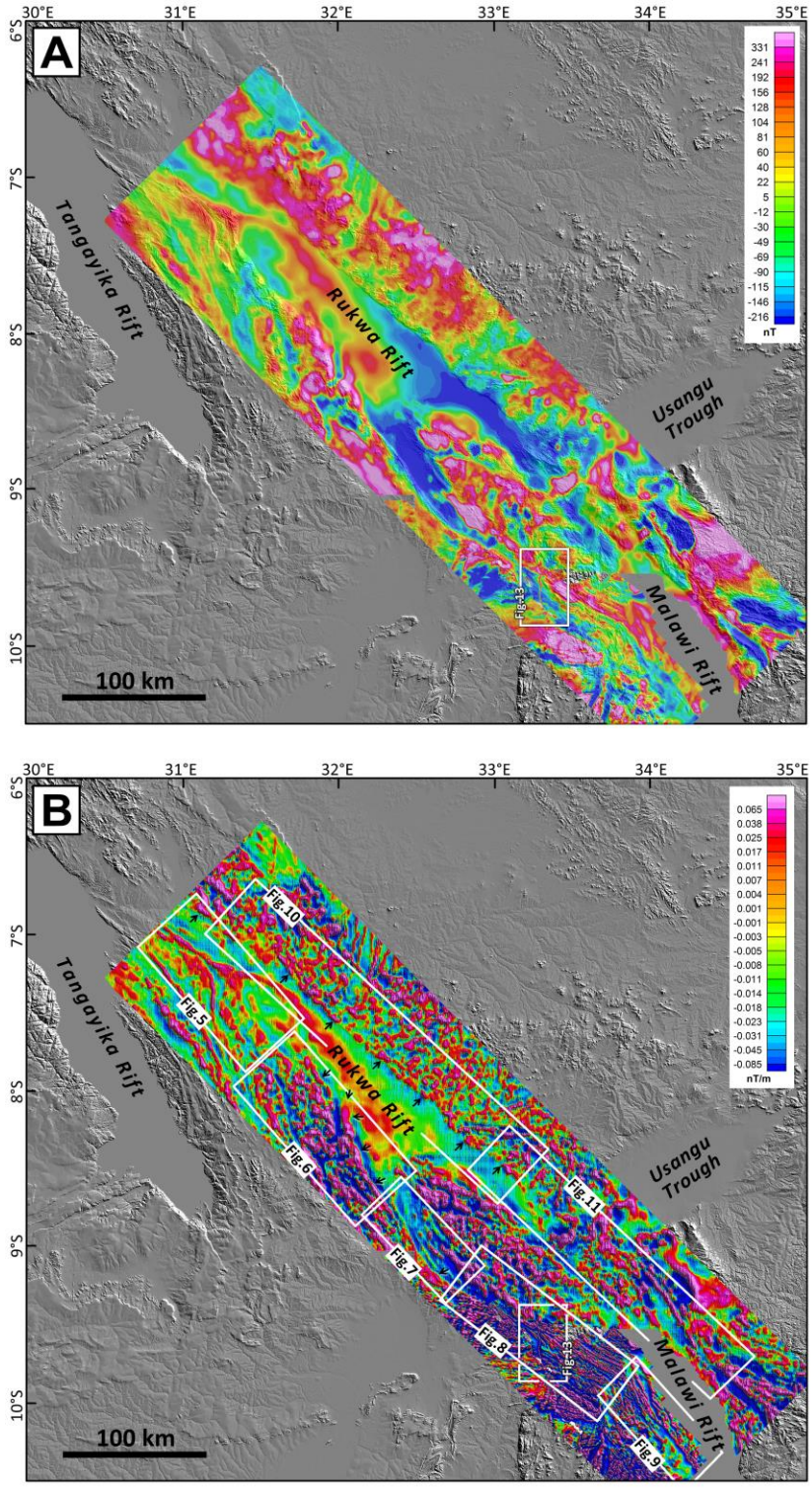

Fig. 4. (A) The reduced to pole Total Magnetic Intensity (RTP-TMI) map of the Rukwa-North Malawi Rift area, draped over the topographic digital elevation model of SW Tanzania. (B) The 1st vertical derivative map of the RTP-TMI map of the Rukwa-North Malawi Rift area draped over the topographic digital elevation model.

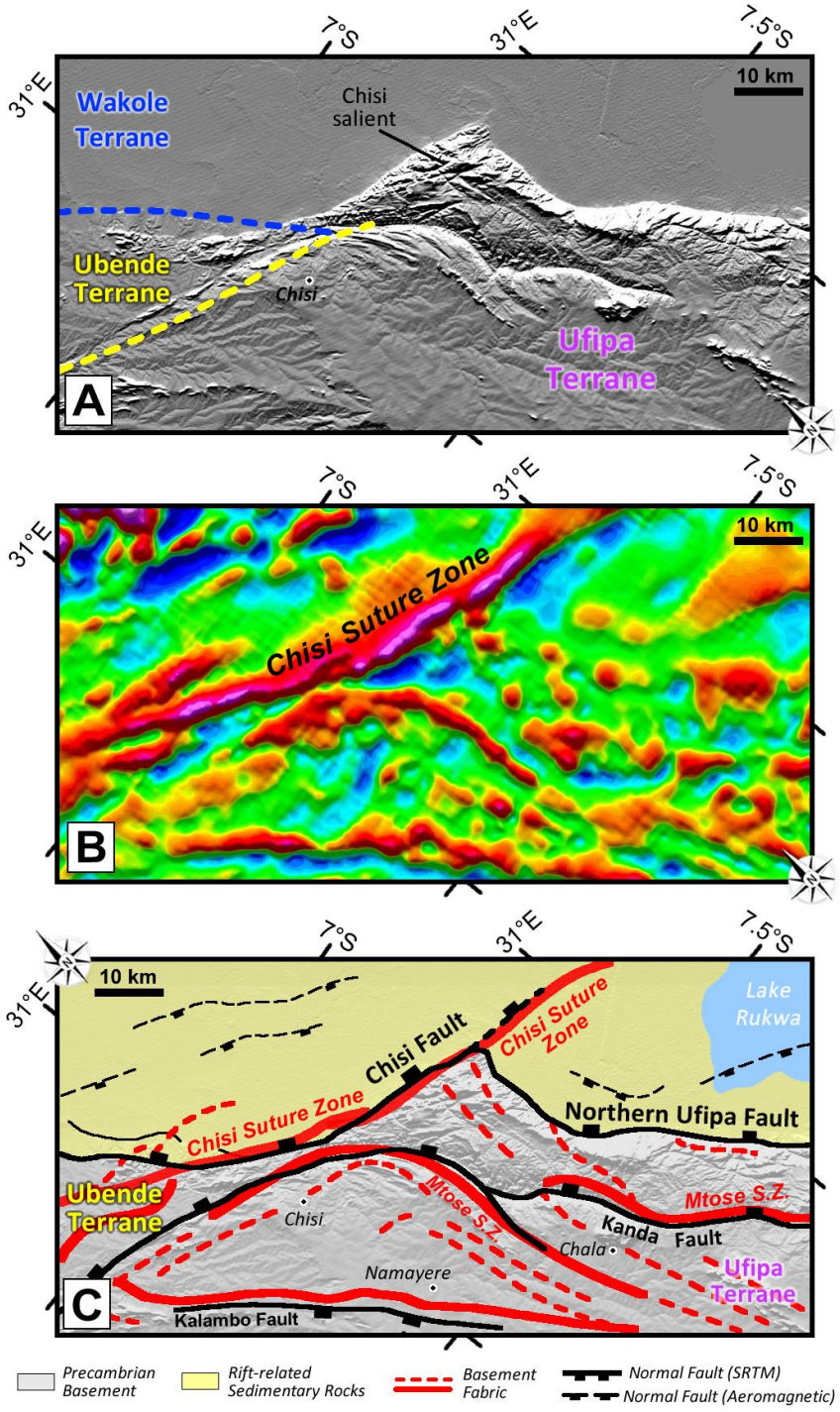

Fig. 5. Northernmost part of the Ufipa Fault, the SW boundary fault of the Rukwa Rift. Topographic digital elevation model in the top panel (A), the vertical derivative of the magnetic data in the middle panel (B), and a structural interpretation in the bottom panel (C).

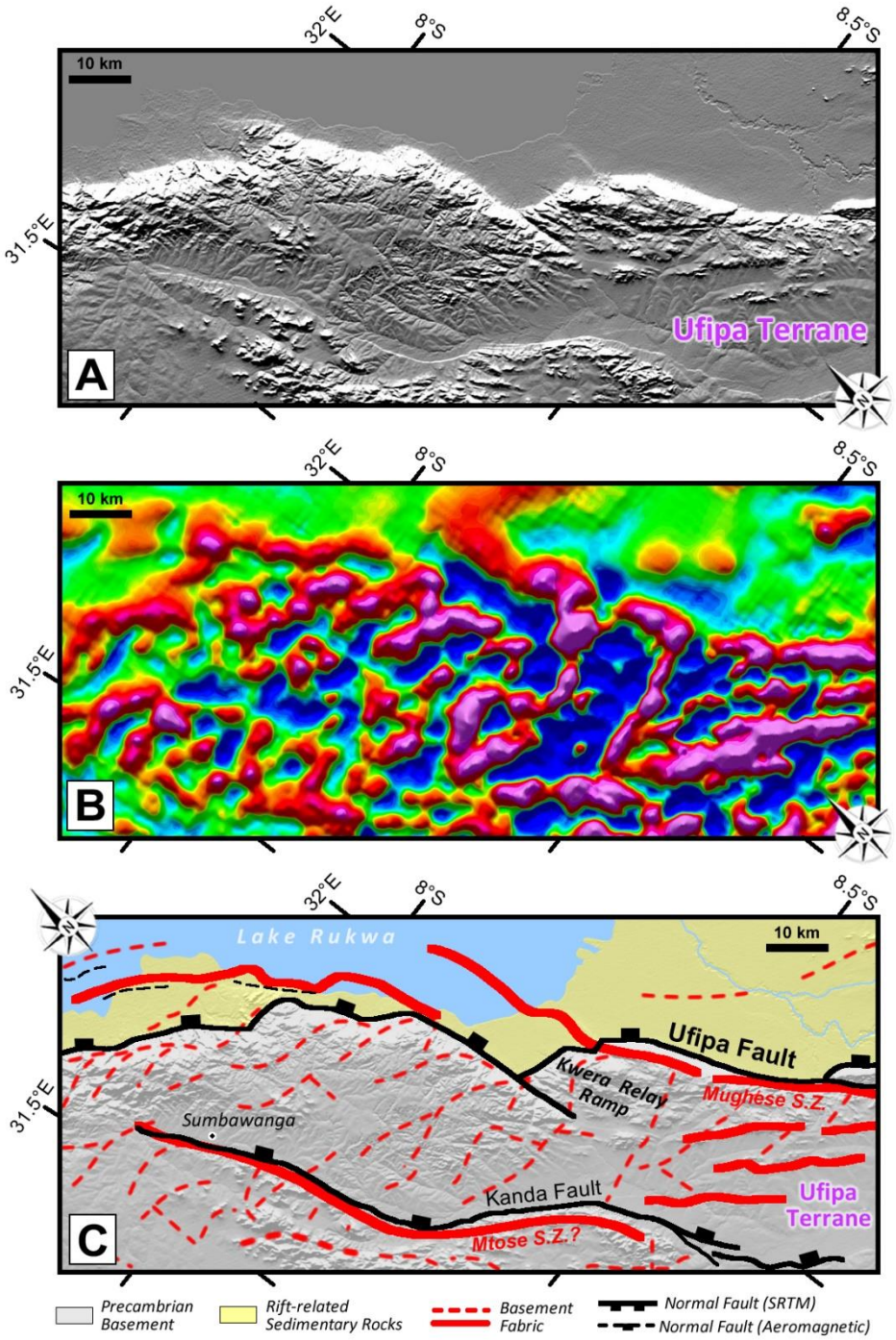

Fig. 6. Central segment of the Ufipa Fault, SW boundary of the Rukwa Rift. Topographic digital elevation model in the top panel (A), the vertical derivative of the magnetic data in the middle panel (B), and a structural interpretation in the bottom panel (C).

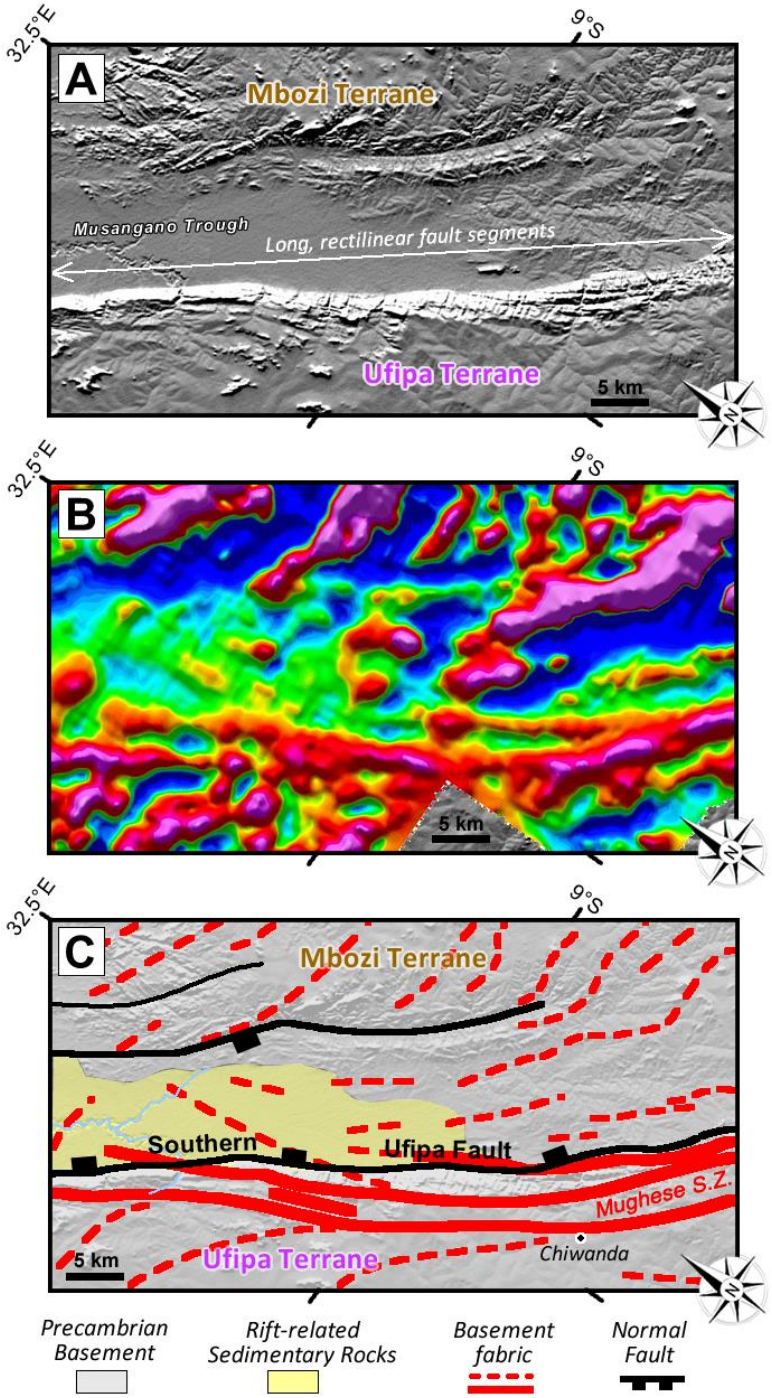

Fig. 7. The Musangano Trough part of the SW boundary of the Rukwa Rift. Topographic digital elevation model in the top panel (A), the vertical derivative of the magnetic data in the middle panel (B), and a structural interpretation in the bottom panel (C).

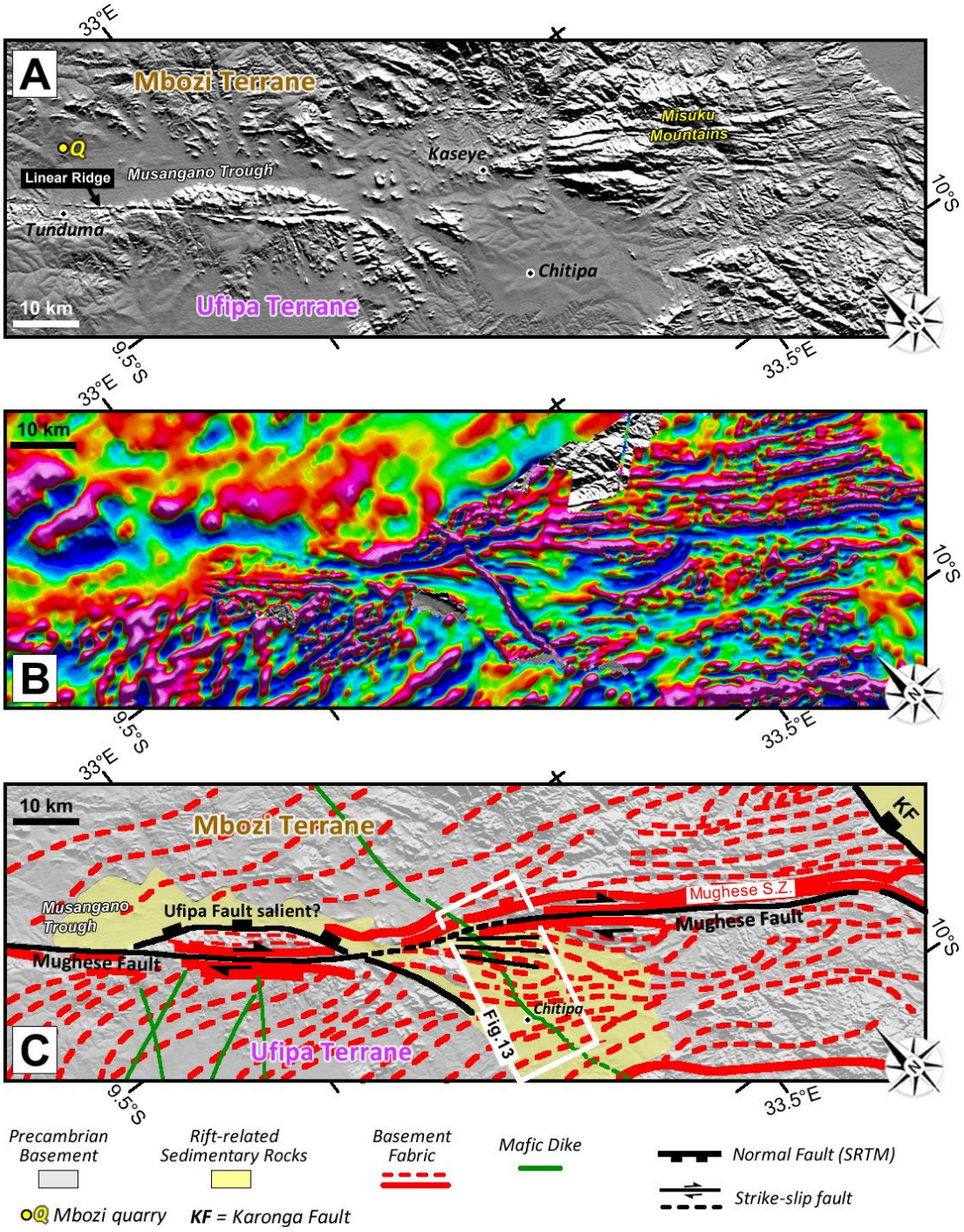

Fig. 8. The SW margin of the Mbozi Block. Topographic digital elevation model in the top panel (A), the vertical derivative of the magnetic data in the middle panel (B), and a structural interpretation in the bottom panel (C).

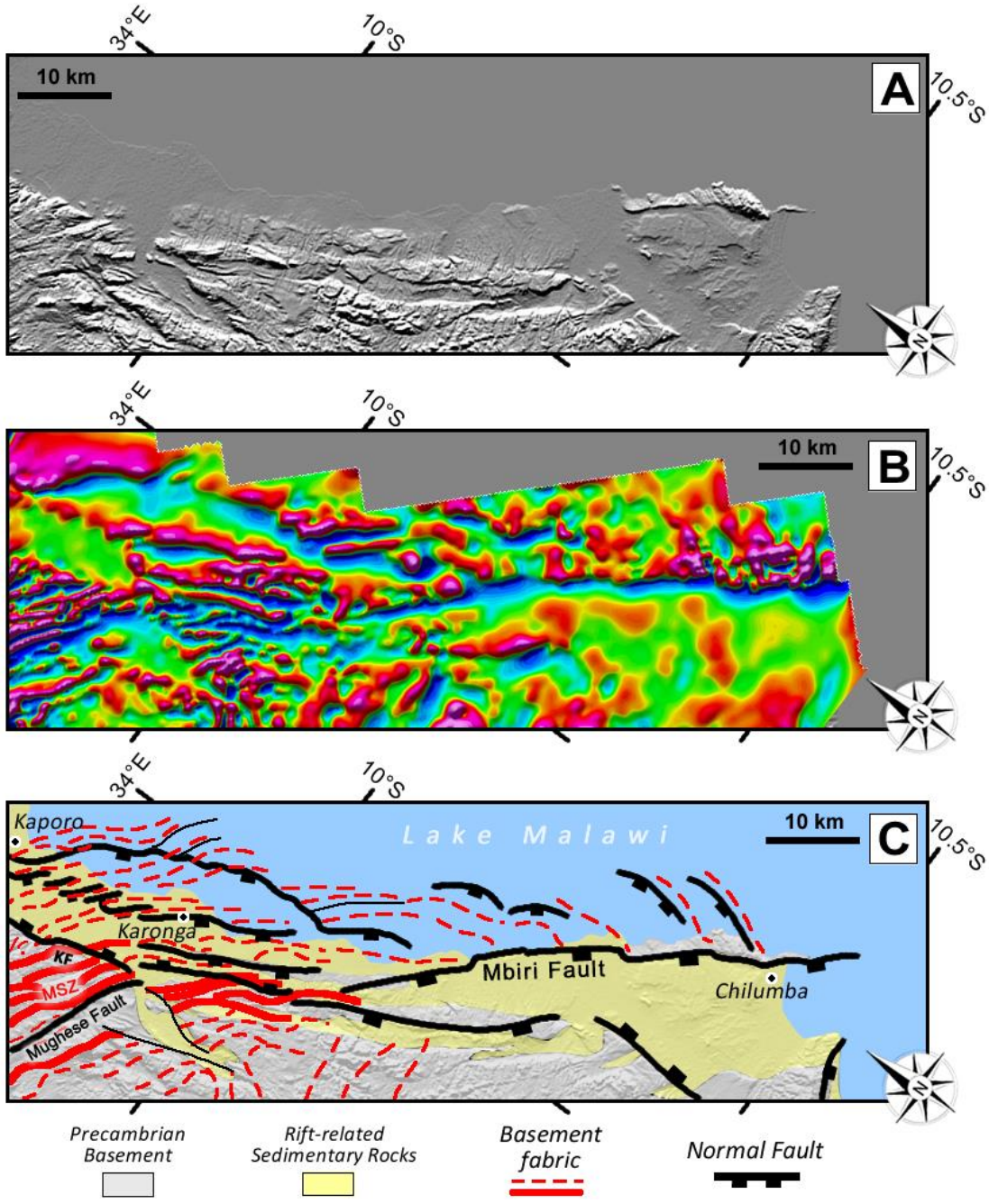

Fig. 9. The SW margin of the North Malawi Rift Basin (Karonga area). Topographic digital elevation model in the top panel (A), the vertical derivative of the magnetic data in the middle panel (B), and a structural interpretation in the bottom panel (C). MSZ = Mughese Shear Zone, KF = Karonga Fault. Fault and basement fabric interpretations from Kolawole et al. (2018).

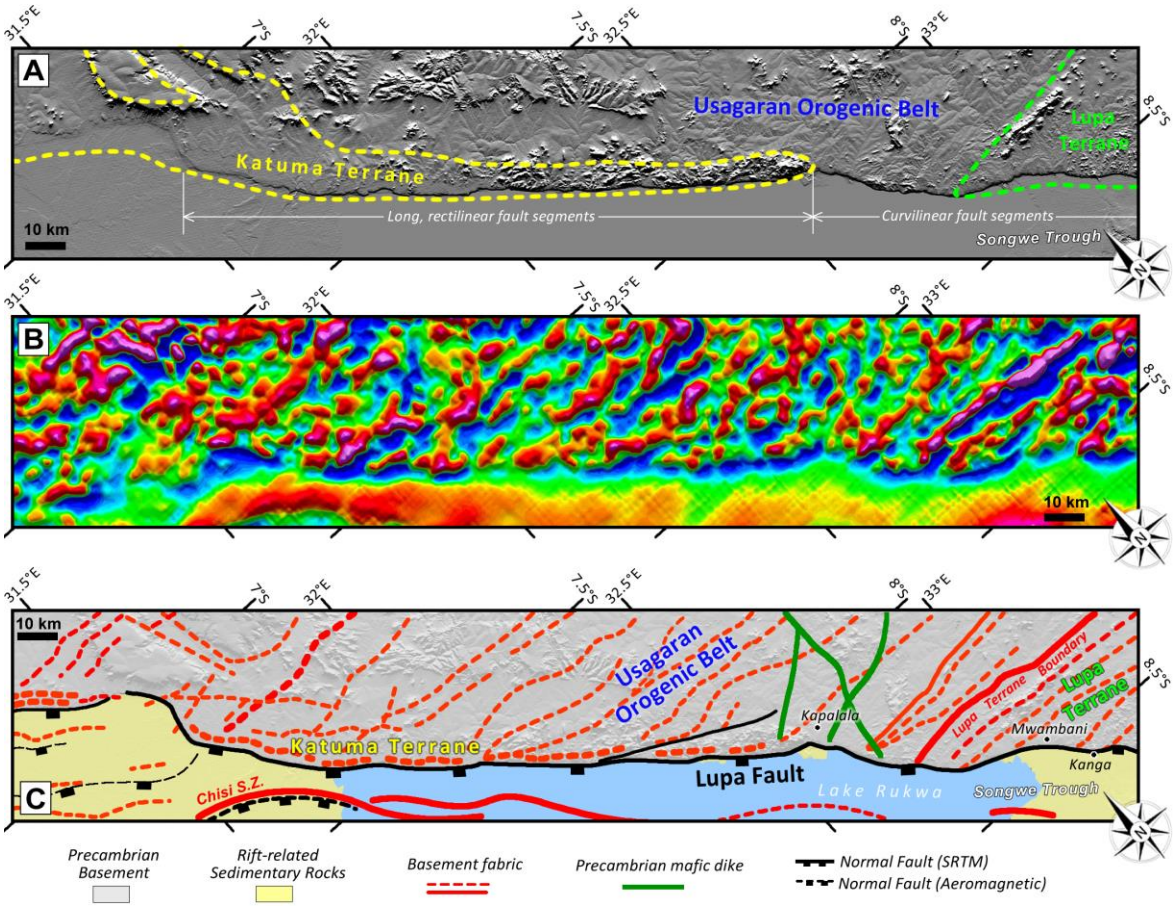

Fig. 10. The northern section of the Lupa Fault, the NE boundary fault of the Rukwa Rift. Topographic digital elevation model in the top panel (A), the vertical derivative of the magnetic data in the middle panel (B), and a structural interpretation in the bottom panel (C).

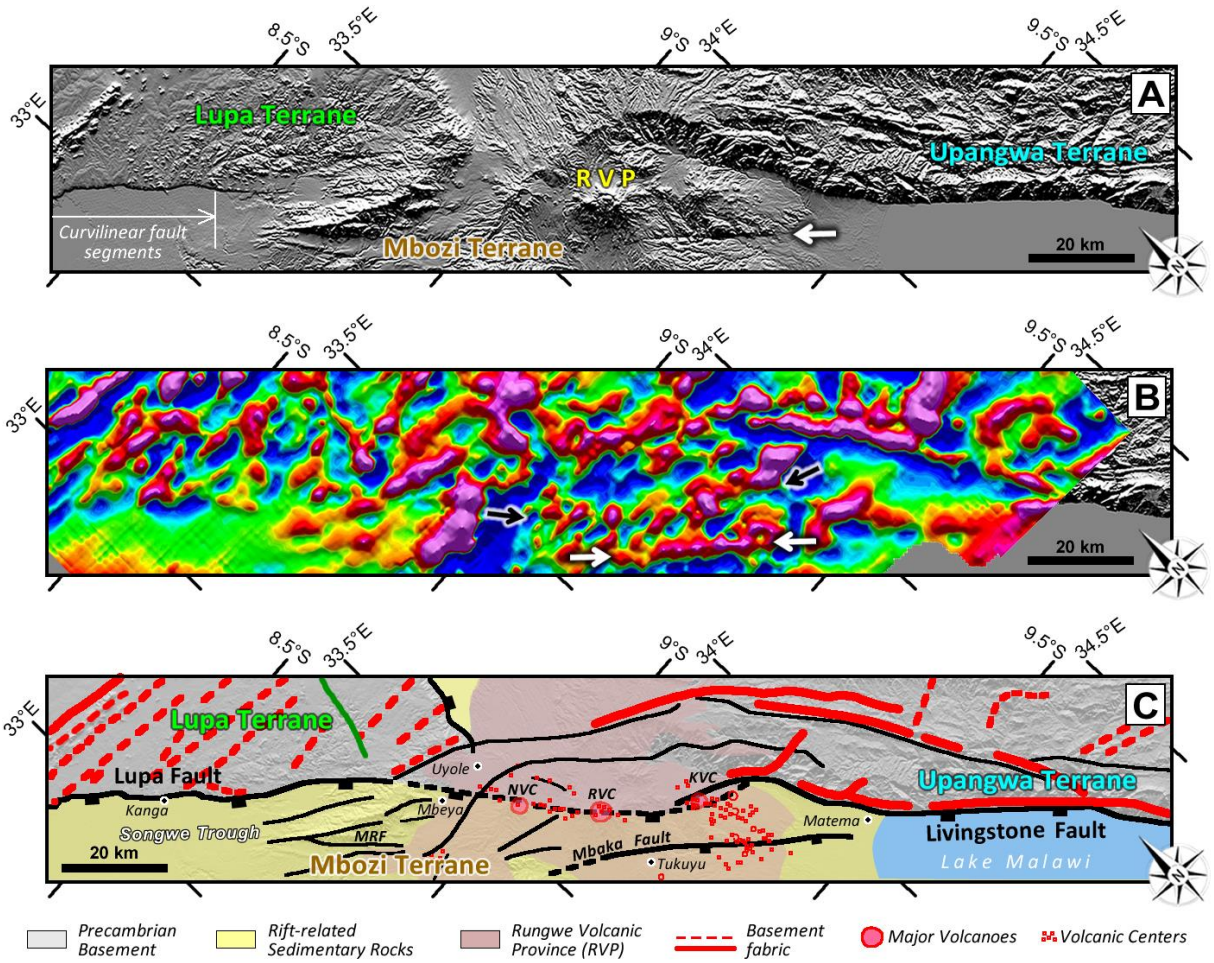

Fig. 11. The southern section of the Lupa Fault, the NE margin of the Mbozi Block (Rungwe Volcanic Province) and a section of the Livingstone Fault (NE border fault if the North Malawi Rift. Topographic digital elevation model in the top panel (A), the vertical derivative of the magnetic data in the middle panel (B), and a structural interpretation in the bottom panel (C). KVC = Kyejo Volcanic Center; NVC = Ngozi Volcanic Center; RVC = Rungwe Volcanic Center. Volcanic centers from Fontijn et al. (2010, 2012).

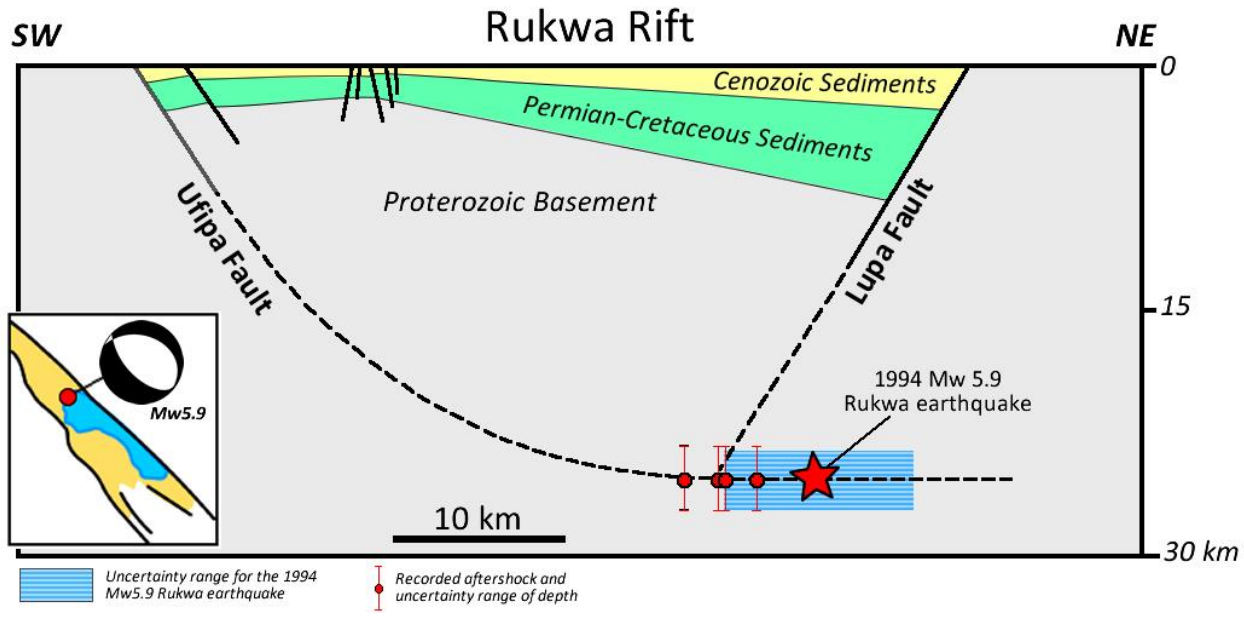

Fig. 12. Generalized geometrical relations of stratigraphic units and normal faults of the Rukwa rift, showing thickening of Cenozoic sediments towards both the Lupa and Ufipa border faults (modified after Zhao et al., 1997).

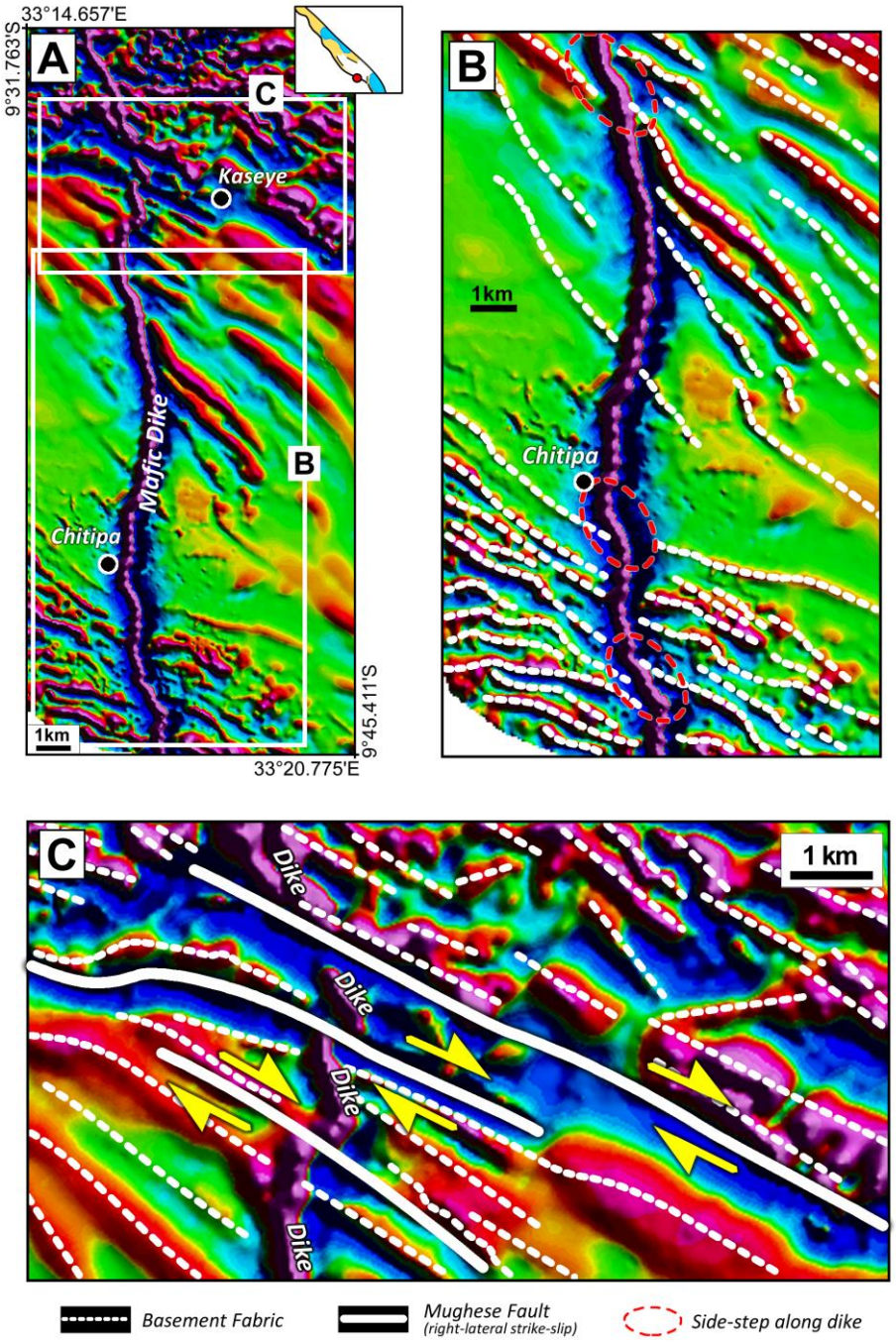

Fig. 13. (A) 1st vertical derivative of the aeromagnetic data covering the Kaseye-Chitipa area along the SW margin of the Mbozi Block (see location in top-right inset map, Figures 4A-B and 8C). (B) Close-up of the central and southern segments of a buried mafic dike (the "Chitipa Dike") showing side-stepping segments that coincide with pre-existing basement fabric. (C) Close-up of the northern segment of the dike showing right-lateral offsets by the continuation of the Ufipa Fault. This strike-slip fault segment is here-in referred to as the Mughese Fault.

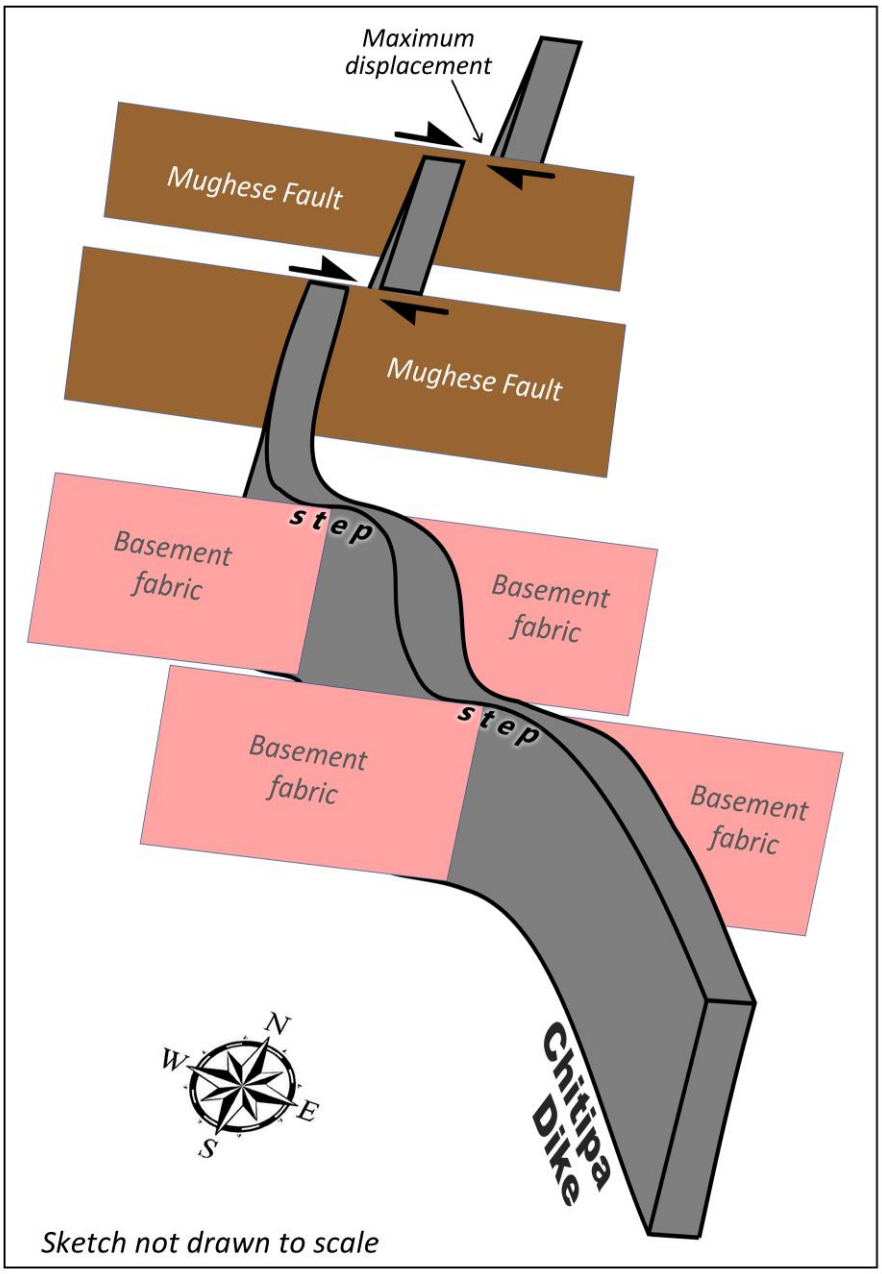

Fig. 14. 3-dimensional (3-D) conceptual model of the geometry of the interpreted dike (the "Chitipa Dike") and its interactions with the pre-existing basement fabric and the post-emplacement Mughese strike-slip fault offset.

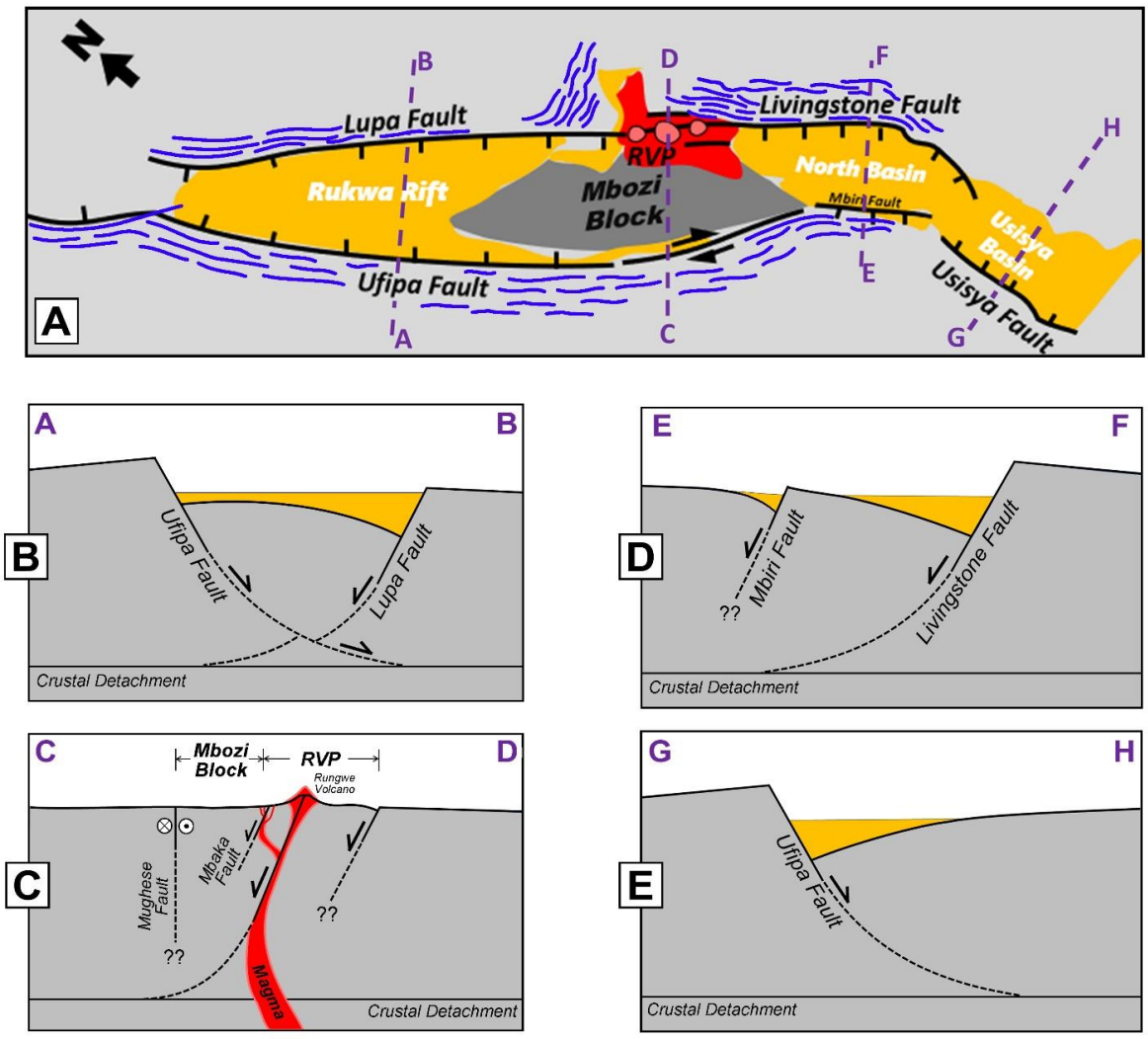

Fig. 15. (A) Generalized cartoon (map view) of the Rukwa-North Malawi Rift Segment (RNMRS) illustrating the continuous structural connectivity along the northeast and southwest boundaries, guided by the basement fabric. Black solid line = fault, blue solid line = basement fabric. RVP = Rungwe Volcanic Province. (B-E) Cross-section cartoons across the segments of the RNMRS, illustrating the possible subsurface geometries and interactions of the domain-bounding structures. LLF = Livingstone-Lupa Fault.

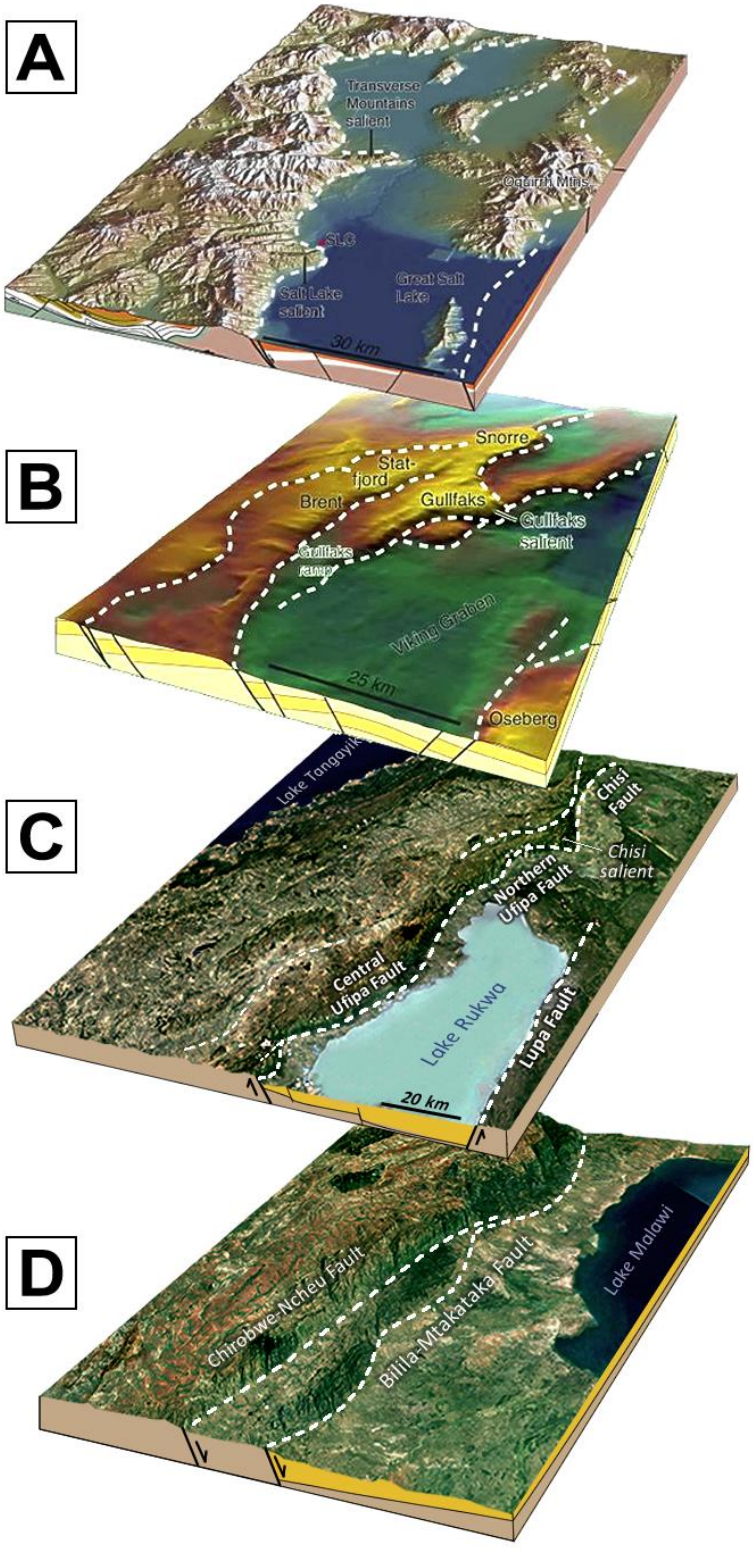

Fig. 16. (A-B) The Wasatch Fault in the Salt Lake area, Utah, and the first-order faults in the northern North Sea (base Cretaceous unconformity) showing concave-curvilinear fault geometries (modified after Fossen and Rotevatn, 2016). (C) Strikingly similar Concave-curvilinear fault geometry occurs in the northern Ufipa Fault and Chisi Fault in the Rukwa Rift. However, the Central Ufipa Fault shows convex-curvilinear fault geometry. (D) The Bilila-Mtakataka Fault also shows excellent convex curvilinear fault geometries.

1581

1582

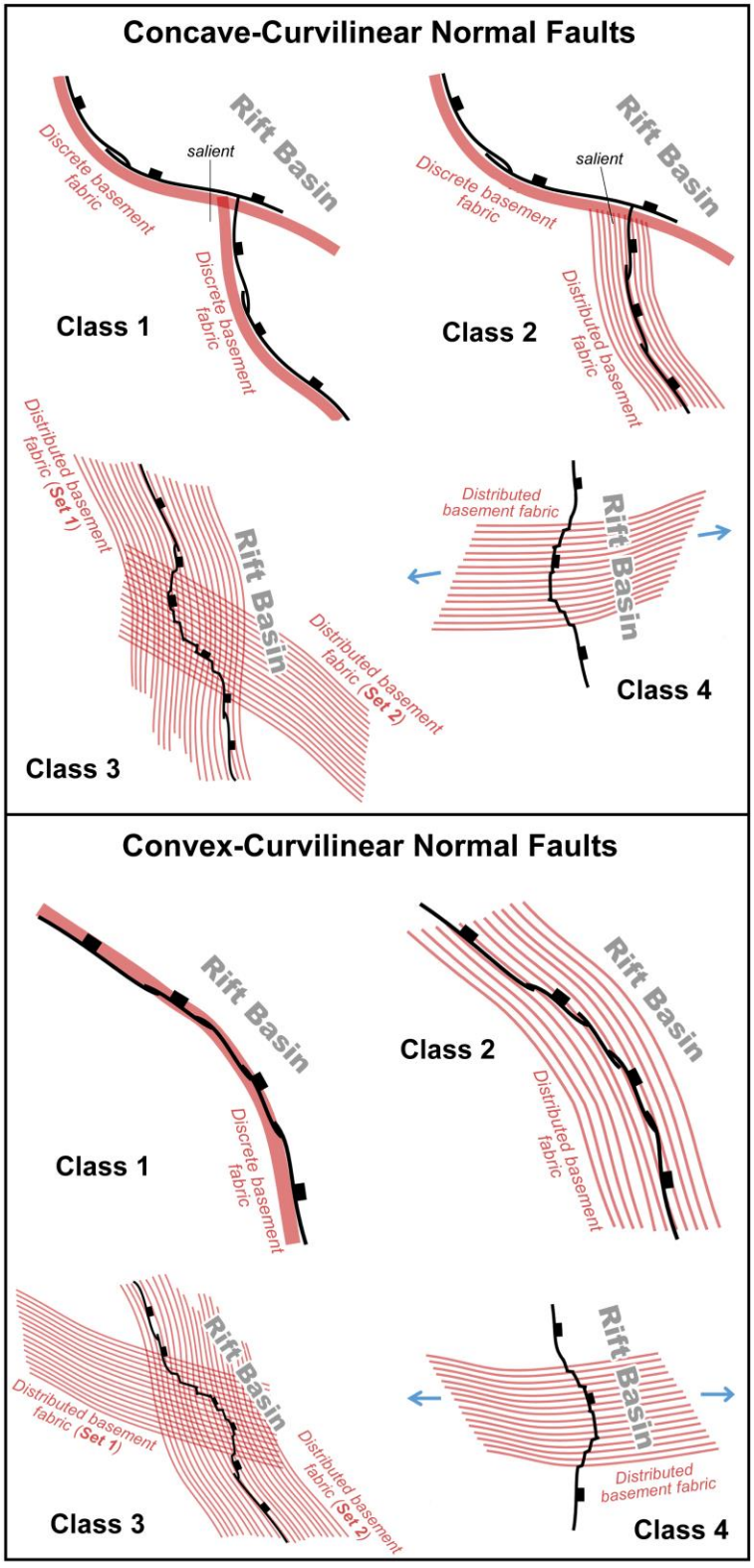

Fig. 17. Models illustrating the control of varying configurations of pre-existing basement fabrics on the development of concave- and convex-curvilinear normal fault plan-view geometries. These models are based on the observations from the Rukwa – North Malawi Rift Segment (this study).

1609

1610

1611

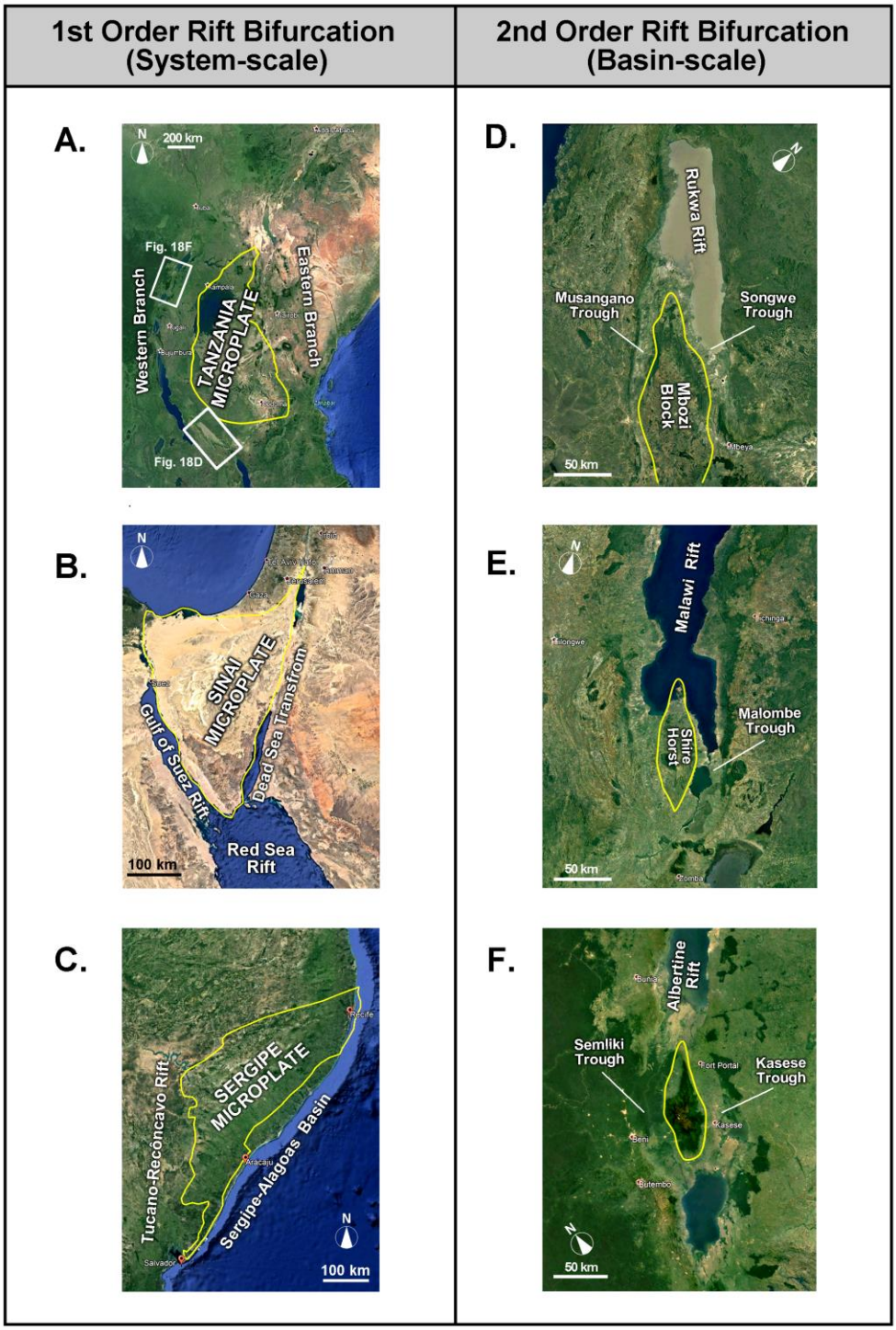

Fig. 18. Examples of system-scale rift bifurcation in the (A) East African Rift System, (B) Red Sea Rift and (C) South Atlantic Rift; and examples of basin-scale rift bifurcation in the (D) Rukwa Rift (see Fig. 18A for location), (E) southern Malawi Rift and (F) Albertine Rift (see Fig. 18A for location). These examples show that the 2nd order bifurcations are integral components of inter-rift transfer zones where the coupling of rift segments take place.